공학박사 학위논문

Generation of charged SiC nanoparticles in the gas phase and their effects on deposition behavior of homo-epitaxial SiC films during HWCVD process

열 필라멘트 화학 기상 증착 공정 중 형성되는 하전된 실리콘 카바이드 나노입자와 동종에피택시 성장에 이들이 미치는 영향

2020년 8월

서울대학교 대학원
재료공학부

김 다 슬

Generation of Charged SiC nanoparticles in the gas phase and their effects on deposition behavior of homo-epitaxial SiC films during HWCVD Process

지도 교수 황 농 문

이 논문을 공학박사 학위논문으로 제출함
2020 년 7 월

서울대학교 대학원
재료공학부
김 다 슬

김다슬의 공학박사 학위논문을 인준함
2020 년 6 월

위 원 장 주 영 창 (인)
부위원장 황 농 문 (인)
위 원 장 호 원 (인)
위 원 박 진 우 (인)
위 원 정 재 수 (인)

Abstract

Generation of Charged SiC nanoparticles in the gas phase and their effects on deposition behavior of homo-epitaxial SiC films during HWCVD Process

Daseul Kim

Department of Materials Science and Engineering

Graduate School of Engineering

Seoul National University

As demand for high efficiency and high performance of devices used in various fields is increasing, the development of new materials with better functionality and reliability than before is required. Since silicon carbide (SiC) has excellent physical properties such as a wide band gap, a high breakdown field, high thermal conductivity, and high electron mobility, many studies are actively conducted to apply it to power semiconductors, high efficiency LED device, solar cells and so on.

Chemical vapor deposition (CVD) is mainly used to deposit crystalline SiC. Among them, hot wire CVD (HWCVD) is advantageous for low temperature, large area deposition and low maintenance cost in comparison with other CVD techniques.

Meanwhile, non-classical crystallization, which suggests that crystals grow by nanoparticles rather than atoms or molecules, is emerging in the field of crystal growth. Many pieces of research have been conducted about it not only in the liquid phase but also in the gas phase. Many results showed the generation of charged nanoparticles (CNPs) in the gas phase in a variety of CVD processes.

Based on this understanding, deposition behavior of SiC thin films by HWCVD was studied in this study. Above all, SiC nanoparticles were captured for 30 seconds using a shutter and observed by transmission electron

microscopy (TEM).

To confirm that CNPs are generated in the gas phase in CVD process, delay time process was introduced. The size of nanoparticles increased from 2.9 nm to 6.1 nm with increasing the delay time from 0 min to 60 min, which means that the deposited nanoparticles were from vapor phase.

The behavior of nanoparticles generated in HWCVD process was affected by electric field because they are charged. When positive bias was applied to substrates, the number of SiC nanoparticles slightly decreased compared with when no bias or negative bias was applied.

The deposition behavior of SiC films was affected by the applied bias on a substrate holder based on the understanding of theory of charged nanoparticles. A homo-epitaxial SiC film as thick as ~ 200 nm was grown under the substrate bias of – 200 V, whereas polycrystalline SiC films were grown under 0 V and + 15 V. It indicates that nanoparticles generated in the gas phase should be charged.

Also, behavior of nanoparticles depends on many process parameters such as gas concentration, temperature of filaments and so on. When the temperature of tungsten filaments was 2300℃, SiC nanoparticles of 2 ~ 3 nm were captured. When the temperature was lowered to 2000℃, however, SiC

nanoparticles of ~ 8 nm were captured. When ($SiH_4 + CH_4$)/H_2 was decreased from 0.04 to 0.01, the size of SiC nanoparticles was decreased from 3 to 1 nm. Also, the concentration of nanoparticles decreased with decreasing of the precursor concentration.

In order to observe how the behavior of CNPs changes as additional potential bias was applied to the filaments, nanoparticles were captured with be applied + 50 V, 0 V, - 50 V to the filaments.

When a positive bias applied to the filament, there was no significant difference in the size distribution of nanoparticles from that without bias. When negative bias was applied to filaments, whereas, no nanoparticles ware observed as compared with when no bias or positive bias was applied.

According to non-classical crystallization, size of nanoparticles affects liquid-like property of them. If the nanoparticles are small, they become liquid-like, and vice versa. Based on this understanding, it was studied whether homo-epitaxial growth is possible by controlling the behavior of CNPs. When nanoparticles were small enough, an epitaxial SiC film of ~ 100 nm thickness could be grown. When nanoparticles were large, polycrystalline SiC films were deposited.

These results obtained in this study can provide important experimental

evidence that the size and charge of nanoparticles generated in the gas phase play as an important process variable when thin films grow by non-classical crystallization.

Keyword : Silicon carbide, Hot wire chemical vapor deposition, Non-classical crystallization, Thin film growth, 4H-SiC

Student Number : 2013-23035

Table of Contents

List of Figures

CH_4)/H_2 of 0.04, (c) with the bias of – 50 V and the gas ratio of (SiH_4 + CH_4)/H_2 of 0.04, (d) with the bias of – 50 V and the gas ratio of (SiH_4 + CH_4)/H_2 of 0.01, and (e) with the bias of – 50 V, the gas ratio of (SiH_4 + CH_4)/H_2 of 0.01 and the distance of 2 mm between the wires and the substrate.

List of Table

Chapter 1. Introduction

1.1. Study Background and Purpose of Study

As demand for high efficiency and high performance of devices used in various fields has been increased, the development of new materials with better functionality and reliability than before is required. Since silicon carbide (SiC) has excellent physical properties such as a wide band gap, a high breakdown field, high thermal conductivity, and high electron mobility, many studies are conducted to apply it to power device, high efficiency LED device, solar cells and so on.

Besides, due to limitation for physical properties of silicon (Si), there is a demand for materials to replace Si in electronic devices that require high frequency, high voltage, high temperature operation, etc. SiC, gallium nitride (GaN) and diamond are attractive candidates for replacing Si. Among them, SiC has been actively studied because of its superior thermal properties, production cost and breakdown voltage compared with the other materials [1]. Figure 1 shows materials properties of Si, SiC, and GaN. Fabricating electric devices using SiC can greatly reduce the volume and weight of the system, increase operation speed and reliability, and decrease the power loss [2].

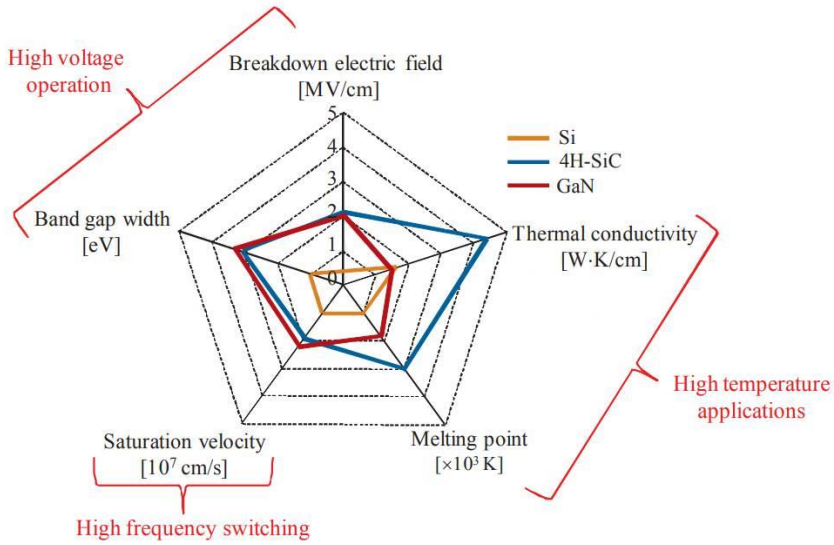

Figure 1. Summary of Si, SiC, and GaN relevant material properties.

By Courtesy of Deblecker et al. [1].

SiC also well known for a materials exhibiting polymorphism called polytypism. More than 250 polytypes are observed in SiC [3]. SiC polytypes are divided by the stacking sequence of the Si-C bilayer. The most common types among SiC polytypes are the cubic (C-), the hexagonal (H-), and the rhombohedral (R-) crystal structures. It could be explained by the different stacking sequence of a close packed structure in the (0001) plane.

The A denoted black dots in Figure 2(a) indicates A layer. B and C denote two different layer, which rotate 60° to each other. Crystal structures of different polytypes can be expressed using the stacking sequence. For example, 3C-SiC has stacking sequence of ABCABC…, 4H-SiC has sequence of

ABACABAC…, and 6H-SiC has sequence of ABCACBABCACB…, where the capital letter stands for the symmetry of crystal and the number indicates periodicity.

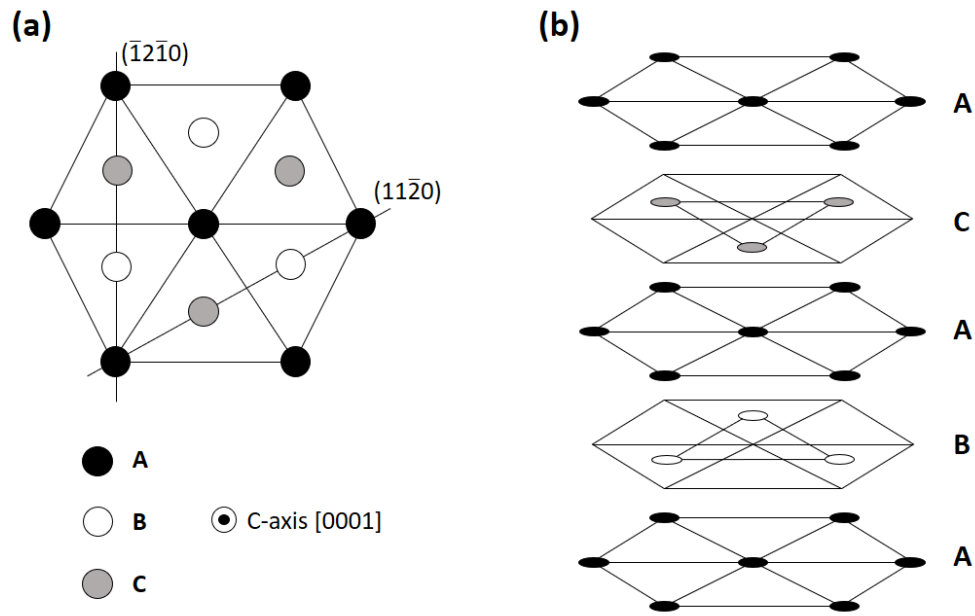

Figure 2. (a) Close packed structure of silicon carbide in (0001) plane. Three different stacking sequences are denoted A, B and C. (b) Stacking sequence of 4H-SiC.

Among various polymorphs of SiC, 4H-SiC is most actively studied for power devices because it has wider band gap than that of 3C- or 6H- SiC. In addition, 4H-SiC wafer is well commercialized up to a size of 150 mm, it has a relatively commercial advantage [4].

SiC films are usually grown using chemical vapor deposition (CVD) methods. Among the CVD methods, crystalline SiC films deposited using hot wire CVD (HWCVD) are mainly used for a window layer of solar cells, color sensors and thin film transistors [5-9].

HWCVD, also called Cat-CVD (catalytic-CVD), take place upon decomposition temperature of reactant or precursor gases at a surface of hot filament which is resistively heated at temperature. HWCVD offers some features that overcome some of the plasma enhanced CVD (PECVD) limitations, which is mostly used deposition technique in the industry: high deposition rates, absence of ion bombardment during deposition, scalability to larger areas and low maintenance costs.

Based on the understating of non-classical crystallization, some studies conducted using HWCVD. Non-classical crystallization is a theory that suggest a new paradigm of crystal growth in liquid or gas phase. Hwang and his colleagues [10-14] proposed 'the theory of charged nanoparticles (TCN)', which suggests that CNPs are spontaneously generated in the gas phase during synthesis of nanostructures using CVD or some physical vapor deposition (PVD) systems and that CNPs become building blocks of nanostructures (This will be described in detail in Chapter 1.2.).

In HWCVD, negative or positive current was measured by Song et al. [15] for reasons such as electron emission [16] due to a metal heated to high

temperature, surface ionization [10, 17], collision and ionization between electrons and gases [15], and etc. In addition, nanoparticles generated by ion-induced nucleation [18] or photo induced nucleation [19] could be charged by gaining or losing electrons.

The fact that enough CNPs are generated in the gas phase during process is experimentally confirmed by Lee et al. [20] and Hong et al. [21, 22] in silicon HWCVD system, and Jeon et al. [23, 24] and Park et al. [25] in diamond HWCVD system.

Also various studies have been conducted using HWCVD based on TCN, such as success of epitaxial silicon thin film growth at low substrate temperature by controlling the CNPs by Jung et al. [26].

Some studies have been reported on the epitaxial growth of SiC films using HWCVD. Zhiyong et al. [27] and Hens et al. [28] reported epitaxial growth of 3C-SiC on a silicon. Also 3C-SiC deposition on SiC substrate was reported by Robbins and Seman as a patent [29]. Van Zeghbroeck et al. [30] showed a homo-epitaxial growth of 4H-SiC. These researched explained growth behavior based on the classical crystallization or could not suggest proper principles of the epitaxial growth. However, it turned out that nanoparticles are generated in the gas phase of many HWCVD and they contribute to the film growth. SiC films growth by nanoparticles in HWCVD process is highly probable in the concept of non-classical crystallization.

As described above, it was confirmed that charged nanoparticles generate in the gas phase of CVD and some PVD systems, and that they affect the deposition behavior of thin films and nanostructures. The purpose of this study is to identify charged SiC nanoparticles in the gas phase during HWCVD processes based on the TCN. For that, I examined whether SiC nanoparticles are generate in the gas phase of HWCVD process and it is possible to epitaxial growth of SiC films by controlling these SiC nanoparticles. Firstly, SiC nanoparticles generation in the gas phase of HWCVD was experimentally examined. Secondly, it was confirmed that the behavior of SiC nanoparticles with various process variables and how they affect the crystallinity of the SiC films based on the presumption that these nanoparticles are electrically charged.

1.2. Non-classical Crystallization

1.2.1. Non-classical Crystallization

1.2.1.1. Introduction

From the viewpoint of classical crystallization, it is believed that the growth of thin films and nanostructures occurs at the atomic or molecular level. However, there are many experimental results that cannot be explained in

terms of classical crystallization. These results were explained by some scientists in a non-classical view that building block of nanoparticles is a unit of crystal growth. This new concept is dramatically different from the understanding of classical crystallization. Due to the development of experimental measurement technique such as transmission electron microscopy (TEM), experimental results demonstrating non-classical crystallization have been observed in many systems. The studies of non-classical crystallization have increased dramatically over the past few decades [31-37].

The classical crystallization and the non-classical crystallization are compared in Figure 3 [38]. Figure 3(a) shows the classical crystallization pathway. Once the size of the primary building blocks reaches to a certain size, the building blocks can grow continuously into macro crystal by the layer-wise deposition of individual atoms/ions/molecules on the crystal surface. However, Figure 3(b) shows a typical way in which non-classical crystallization occurs. An iso-oriented crystal can grow when the oriented aggregation occurs among the primary nanoparticles. Then, this iso-oriented crystal become to single crystals by fusion of nanoparticles. When the surface of these initial nanoparticles is covered with organic components, they can form a mesocrystal via mesoscale assembly (Figure 3(c)). Antonietti and Cölfen [35] studied a mesocrystal considering them as a crystal superstructure. Mesocrystal intermediates can form single crystals by fusion with involved

organic additives. Also when these mesocrystal intermediates are heated to a sufficient temperature, they form a single crystal.

The both of kinetic path in Figure 3(b) and (c) describes the non-classical growth of a crystal, however, when the kinetic path of crystallization follows the path of Figure 3(b), the final crystal is indistinguishable from the crystal grown at the atomic level. This is why the non-classical crystallization has not been well accepted in the crystal growth community.

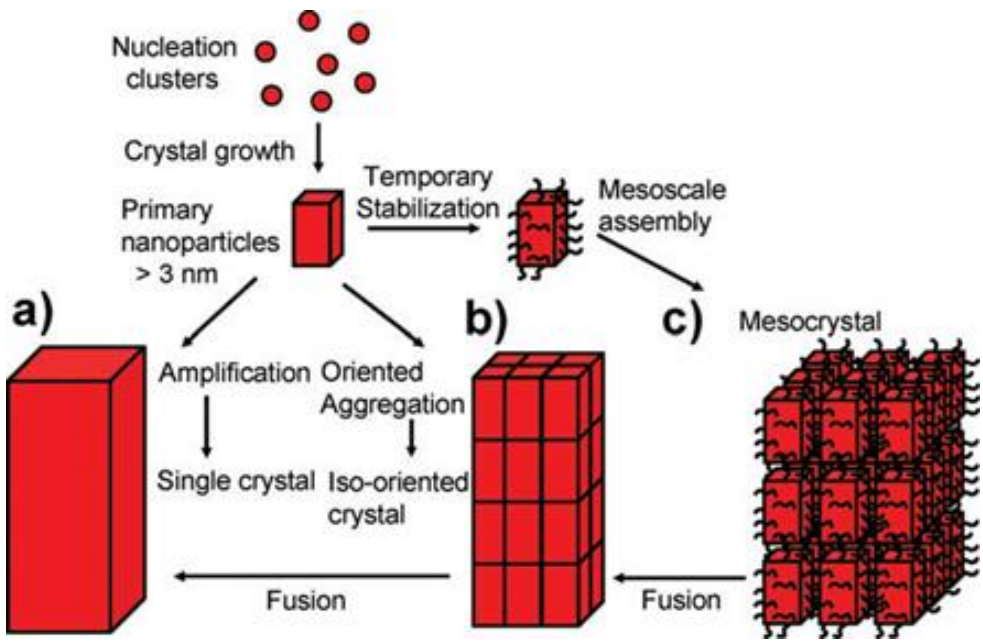

Figure 3. Schematic representation of classical and non-classical crystallization. (a) Classical crystallization. (b) oriented attachment of primary nanoparticles. (c) mesocrystal formation via self-assembly of primary nanoparticles covered with organics. By courtesy of Niederberger and Cölfen [38].

Glasner and his colleagues [39-42] proposed a similar concept to the present non-classical crystallization more than 40 years ago. They suggested that the nanometer-sized nuclei are the building block of KBr and KCl crystal in the presence of Pb^{2+} in aqueous solution. Also, Sunagawa [43, 44] suggested a concept similar to his theory, which the growth building block of diamond is not atoms, or molecules. However, their studies has not attracted much attention at that time.

Recently, the non-classical crystallization has become established. A few books [12, 45-48] have been published and a tutorial and technical sessions had taken place respectively in the spring meetings of Materials Research Society (MRS) and European Materials Research Society (EMRS) in 2014.

1.2.1.2. Observation of Non-Classical Crystallization

As previously described, the advances of experimental techniques have led to the provision of meaningful evidences of the non-classical crystallization. Especially, the in-situ TEM observation makes non-classical crystallization confirmed. Yuk et al. [49] used atomic-level resolution imaging techniques to determine how Pt crystals grow under electron beam radiation. They used

graphene liquid cells to make colloidal Pt nanoparticles as small as 0.1 nm discernable to track their motion [50] and set the electron beam conditions as follows. The microscope is operated at 80 kV with a beam intensity of 10^3 to 10^4 A/m^2 maintained during nanocrystal growth. Upon locating a liquid pocket on the TEM grid, the beam intensity is optimized, which reduces the Pt precursor and initiates nanocrystal growth [50]. Figure 4 shows a TEM image of the nanocrystals connected to the neck in the early stages of coalescence. Neck growth occurs simultaneously with decreasing length (l) and thickness (t), which means that atoms travel to the neck by surface diffusion. After coalescence, the nanocrystal structure is gradually reorganized to evolve the truncated surface. This also means that crystal growth is caused by nanoparticles. Considering that this experiment took place at a low temperature of 23°C [49], such low temperature liquid-like coalescence does not occur when neutral particles are generated.

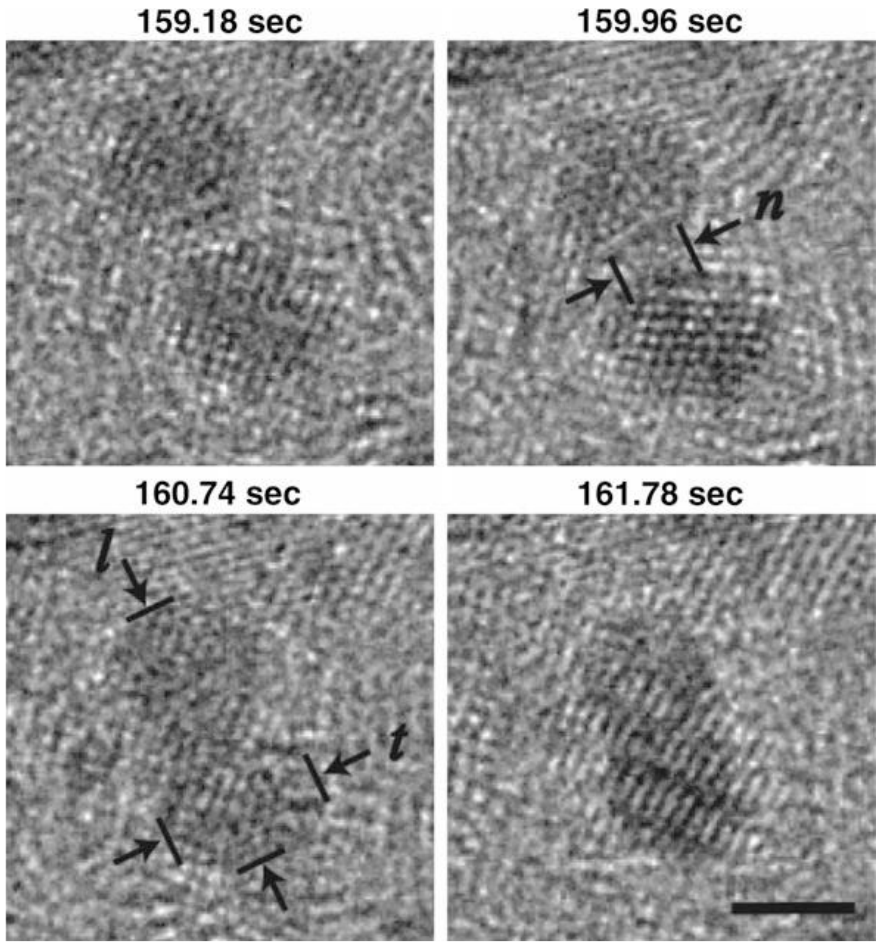

Figure 4. Pt nanocrystal dynamics of coalescence. l, t and n in the figure represent respectively the length along the center-to-center direction, the thickness in vertical direction to the length and the neck diameter. Scale bar, 2 nm. By courtesy of Yuk et al. [49].

Tang et al. [51] observed spontaneously with CdTe nanowires when organic stabilizers on the surface of CdTe nanoparticles were removed. The nanowires in Figure 5 were grown by CdTe nanoparticles of 3.4 nm and 5.4 nm, respectively, and the diameter of the final nanowire was the same as the

size of the initial particles. They explained that this self-organization is due to the strong dipole-dipole action, and by examining the aliquots of the dispersions in the early stages of nanowire formation, it is proven that the nanoparticles are the building blocks of the nanowires of Figure 5. This result implies that the nanoparticles are also involved in nanowire growth and are evidence of non-classical crystallization.

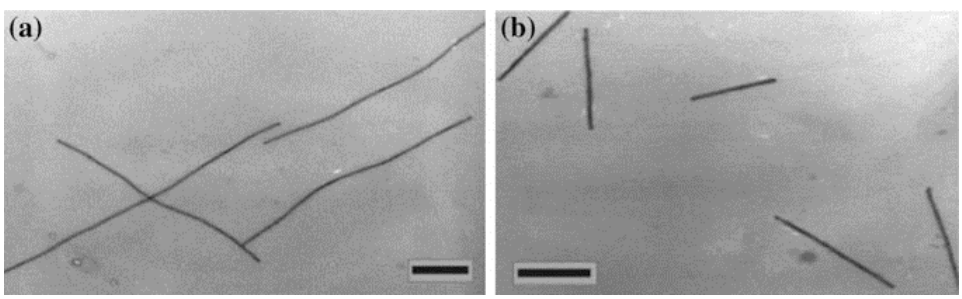

Figure 5. TEM images of CdTe nanowires made from (a) 3.4 nm and (b) 5.4 nm of nanopartiles. Scalebars, 100 nm. By courtesy of Tang et al. [51].

The formation of nanowires or necklace nanocrystal chains via the oriented attachment of nanoparticles has been reported for various materials such as Au, Ag, TiO_2, ZnS, CdTe, PbSe, ZnO and SnO_2 [32]. The formation mechanism would be similar to other nanostructures such as nanodendrites, nanoleaves and nanomultipods because these were also suggested to be synthesized by the oriented attachment of nanoparticles [52-54]

1.2.2. Theory of Charged Nanoparticles

1.2.2.1. Theory of Charged Nanoparticles

Although the classical crystallization based on the TLK model is well established, there are many phenomena, which cannot be explained by the classical viewpoint. A well-known phenomenon is that diamond can grow in a low-pressure synthesis, while graphite is thermodynamically stable. Hwang and his colleagues [10-14] suggested that diamond grow by the clusters generated in the gas phase.

Paradox is experimentally observed in which both diamond deposition and graphite etching proceed simltaneously, although the chemical potential of diamond is higher than that of graphite. Figure 6 can be easily explained this paradox with gas phase generation of diamond nanoparticles [11]. Before the gas phase nucleation, the gas phase is supersaturated and has the driving force to precipitate carbon in both diamond and graphite (Figure 6(a)). However, after the gas phase nucleation, the gas phase is undersaturated and has the driving force to be etched into gas in both diamond and graphite (Figure 6(b)). If the diamond nanoparticles are initially formed in the gas phase and then

deposited on the substrate, the situation of simultaneous diamond deposition and graphite etching is thermodynamically possible.

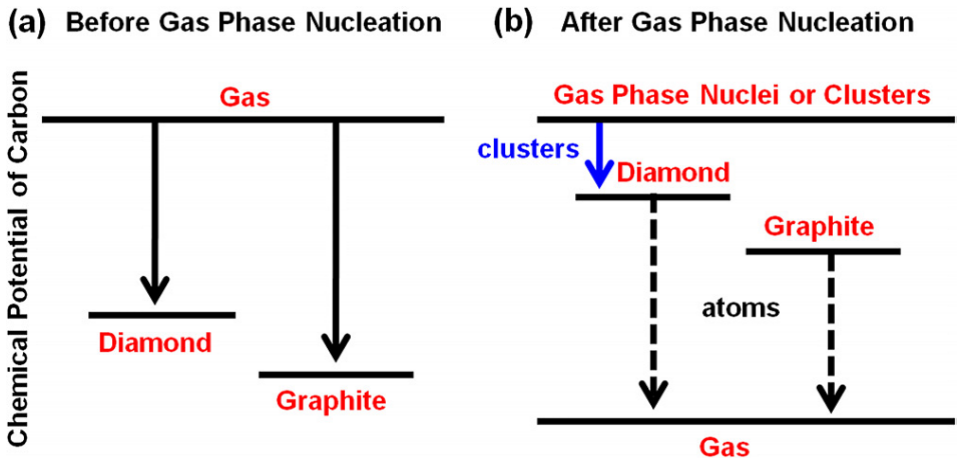

Figure 6. The chemical potentials of carbon in diamond, graphite and the gas phase before (a) and after (b) gas-phase nucleation. The arrows indicate the paradox-free direction of carbon flux. By courtesy of Hwang and Lee [11].

This new mechanism is called 'theory of charged nanoparticles (TCN) [11]' According to this theory, the charge characteristics of the nanoparticles produced in the gas phase play an important role because the charge plays a decisive role in terms of non-classical crystallization [12].

Hwang et al. [55] observed that the deposition behavior on the two substrates was different when silicon and iron substrates were placed at the

same time during the diamond deposition process (Figure 7). When the charged diamond nanoparticles (CNPs) deposit on a Si substrate, the nanoparticles form a dense diamond film (Figure 7(a)). When CNPs deposit on a Fe substrate, on the other hand, they form a porous structure called soot (Figure 7(b)). This is because the CNPs lose or maintain their charge depending on the electrical properties of the substrate called charge transfer rate (CTR) which corresponds to the rate of the hydrogen evolution reaction of electrode materials in electrochemistry [56]. Iron has the higher CTR than silicon. Therefore, the nanoparticles deposited on the iron substrate are more likely to lose their charge than when deposited on silicon. When the nanoparticles are charged, they have liquid-like properties, which contribute to the formation of porous or crystalline deposits (This will be treated in Chapter 1.2.2.2).

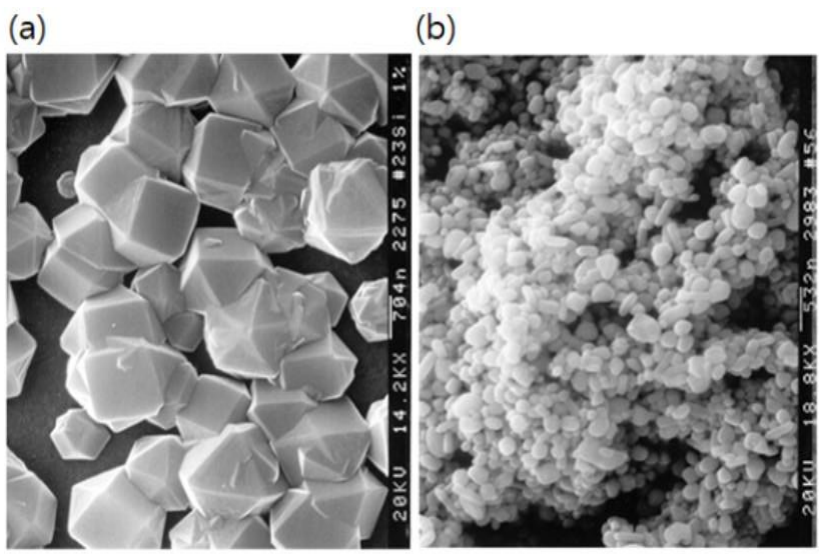

Figure 7. SEM image of deposited (a) diamond on a Si substrate, (b) soot

on an Fe substrate. By courtesy of Hwang et al. [55].

Hwang et al. [55] also observed that the deposition behavior changed by simply grounding or floating the Fe substrate during the diamond deposition process. After 2 hours of deposition, the grounded and floated Fe substrates were observed (Figure 8). Soot grew on the grounded substrate. On the other hand, on a floated Fe substrate where a quartz was placed under the Fe substrate, soot was first created and diamonds grew up on it. As mentioned above, it can be seen that the deposited diamond building blocks grow into diamond film if they keep their charge on the substrate, and vice versa, soot. In other words, these results suggest that charge plays an important role not only in stabilizing diamond but also in liquid-like clusters so that it can epitaxially fuse on the growing surface.

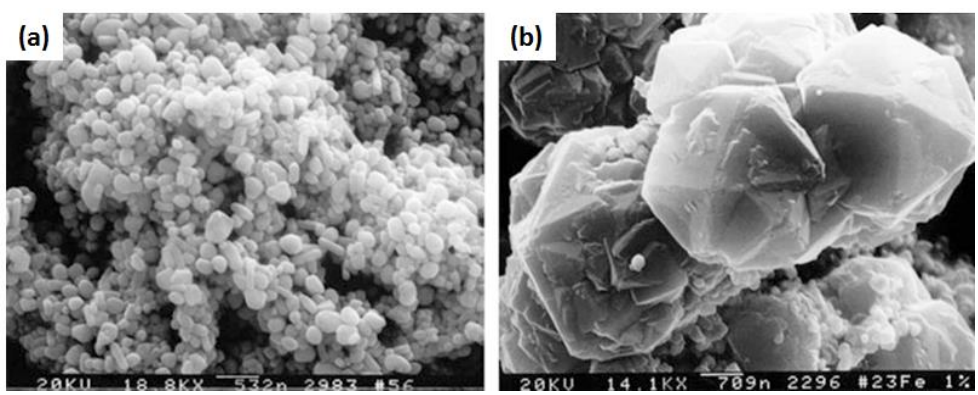

Figure 8. SEM image of deposited (a) soot on a grounded Fe substrate,

(b) diamond on an initially-formed soot on a floating Fe substrate. By courtesy of Hwang et al. [55].

According to the TCN, CNPs are spontaneously generated and some of them are charged in the gas phase of most CVD processes and they become the building blocks of thin films and nanostructures. If nanoparticles are neutral, they undergo random Brownian coagulation. If nanoparticles are charged, however, they deposit as dense films without forming voids. This is why CNPs are liquid-like and undergo self-assembly.

1.2.2.2. Effect of Charge on the Bond Strength

According to TCN, the growth of diamond and silicon crystals is impossible unless the building blocks of CNPs have liquid-like properties [24, 55, 57-59]. As mentioned earlier in Figures 7 and 8, the liquid-like properties of CNPs appear to be due to charging.

Clare et al. [60] studied the difference in bond strength depending on the presence of charge between in the molecules of SiH_4 and Si_2H_6 by ab-initio calculations. They calculated the difference in the energy to break a Si-H bond

in six species: SiH_3, SiH_4, SiH_3^-, SiH_4^-, SiH_3^+, and SiH_4^+. They also did similar calculations on Si-Si bond in the species: Si_2H_6, Si_2H_5, $Si_2H_6^-$, $Si_2H_5^-$, $Si_2H_6^+$, and $Si_2H_5^+$. The results of calculation are shown in Table 1.

Compound	Si-H (eV)	Si-Si (eV)
SiH_4 (optimized)	3.9	-
SiH_4^- (optimized)	0.98	-
SiH_4^+ (optimized)	0.30	-
Si_2H_6 (optimized)	3.5	3.2
$Si_2H_6^-$ (optimized)	1.02	1.11
$Si_2H_6^+$ (optimized)	1.59	1.6
SiH_4^- (unoptimized)	1.35	-
SiH_4^+ (unoptimized)	0.09	-
$Si_2H_6^-$ (unoptimized)	1.34	1.3
$Si_2H_6^+$ (unoptimized)	1.49	1.6

Table 1. The bond strength of Si-H and Si-Si bonds. By courtesy of Clare et al. [60].

According to their calculation, if SiH_4 molecule is negatively charged, the bond strength of Si-H in SiH_4 molecule decreases from 3.9 eV to 0.98 eV, and if SiH_4 molecule is positively charged, it decreases to 0.30 eV. In addition, if Si_2H_6 molecule is negatively charged, the bond strength of Si-H in Si_2H_6 molecule decreases from 3.5 eV to 1.02 eV, and if Si_2H_6 molecule is positively charged, it decreases to 1.59 eV. Further, if the Si_2H_6 molecule is

negatively charged, the bond strength of Si-Si in Si_2H_6 molecule decreases from 3.2 eV to 1.11 e, and if Si_2H_6 molecule is positively charged, it decreases to 1.6 eV.

The charge effect on the bond strength can be explained by the molecular orbital theory. In the molecular orbital theory, the bond order, which indicates the strength or stability of a bond, is the number of bond electron pairs shared by two atoms in the molecule. The order of bonding is defined as half the difference between the number of bonding electrons and the number of anti-bonding electron. This is expressed by the following equation,

$$Bond\ order = \frac{\#\ of\ bonding\ electrons - \#\ of\ antibonding\ electrons}{2} \quad (1)$$

When a nanoparticles is negatively charged, the electrons are added to the anti-bonding orbital, and vice versa, electrons are removed from the bonding orbital when a nanoparticles is positively charged, which weakens the bond strength regardless of the direction of charge.

The weakening of the bond strength by charging means that charge enhances kinetics. From this concept, Clare et al. [60]'s result is not considered in the clusters and in the gas phase, but it supports the enhanced chemical reactions of precursor gases and the better growth of the crystalline

film in plasma CVD processes where the substrate temperature is generally lower than the thermal CVD processes. In the case of the plasma CVD, there are more ions than the thermal CVD. These ions generate many charged molecules, and weakened binding forces even at low temperatures readily decompose the gas precursors. Further, since the gas precursors are easily decomposed in the plasma, it can easily have a higher degree of supersaturation as compared with other CVD. This can lead to nucleation by ions so called ‘ion-induced nucleation’, which remarkably lowers the nucleation barrier.

Iijima and Ichihashi [61] observed the morphology and lattice of gold nanoparticles with about 460 atoms by high resolution TEM (HRTEM) with a time resolution of 1/60 s (Figure 9). The shape of the particle has changed continuously every few tenths of a second. Changes were often accompanied by particle rotation and translation. The internal structure also changed from single crystals to twinned crystals, and vice versa. As the particle size increases above 100 Å, the particle motion slows down and there is little change.

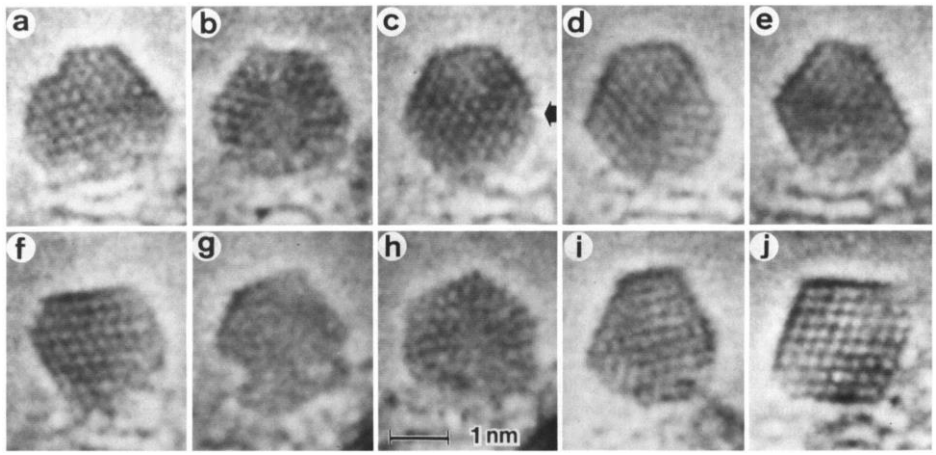

Figure 9. HRTEM images of Au particles of 2 nm size. Microscopic photographs were reproduced from pictures corresponding to a single frame of a video recording tape. The particles in (a), (d), and (i) are single twins. Single crystals with cuboctahedral shape are seen in (e), (f), and (i). From the size of the cuboctahedron (j), the particle theoretically contains 459 gold atoms. The particle also transforms into a multiply twinned icosahedral particle, (b) and (h). By courtesy of Iijima and Ichihashi [61].

They have also studied significant results. The dynamic motion of the nanoparticle changes with the conductivity of the substrate [61]. The Au nanoparticles observed in Figure 9 are on a Si substrate covered with SiO_2. Alumina substrates gave the same results as the SiO_2-covered Si but almost no activities of the clusters were observed when a substrate of α-Fe_2O_3 was used. Also gold particles supported on a gold film remained inactive without undergoing translational motion or structural fluctuation [62]. As the movement of the nanoparticles changes with the electrical conductivity of the

substrate, it can be understood that the nanoparticles are charged by irradiation of the electron beam during the TEM observation. The abrupt structural change described above was attributed to the liquid-like property of CNPs, which called the ‘quasi solid state’ by Iijima and Ichihashi [61].

There are a few processes where the CNPs are contributed to epitaxial growth of films. For example, Yoshida and his colleagues [63-67] studied on the epitaxial growth of films with a nanoparticles by the ‘thermal plasma flash evaporation (TPFE)’ method. In this process, ~ 1 μm size particles are supplied and completely evaporated through the thermal plasma, then precipitated and deposited on the substrate as nanoparticles. These nanoparticles were confirmed to be charged by Hattori et al. [68]. Takamura et al. [64] deposited with the deposition rate as high as ~ 2.2 μm/min of high quality epitaxial high T_c superconducting oxide $YBa_2Cu_3O_{7-x}$ (YBCO) films with T_c = 90 K on the $SrTiO_3$ (100) substrate from clusters of 0.8 nmØ. Since the nanoparticles are charged in the TPFE process and the temperature of the substrate is high, the nanoparticles can be considered to be sufficiently liquid-like to make epitaxial film.

Another method is ‘ionized cluster beam deposition (ICBD)’ proposed by Takagi et al. [69]. The materials to be deposited is placed in a crucible, heated to raise the vapor pressure, and then passed through a small nozzle to form clusters undergoing adiabatic and supersonic expansion [70]. The clusters consist of 500 to 1000 atoms [69, 71], some of which are ionized by impacting

of electrons and then accelerated with a few kV to the substrate. The figure describing this experiment is shown in Figure 10.

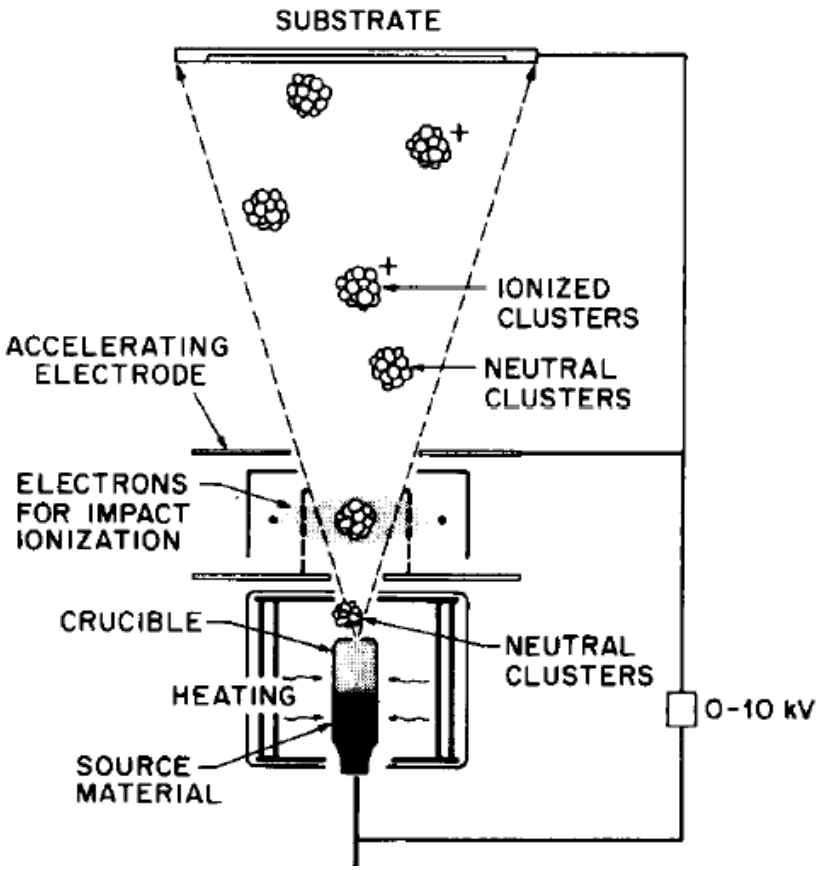

Figure 10. Schematic of ICBD. By courtesy of Brown et al. [72].

Yamada et al. [73] used the ICBD process to accelerate the cluster by an electric field to epitaxially grow aluminum films on Si (111) and Si (100) substrates at low temperatures. This is because charge is an important factor in the ICBD process, and it cannot be epitaxially grown when neutral particles

are accelerated to the same degree of charged particles. In the TPFE process, it appears that the epitaxial film deposition by soft-landing of the nanoparticles without acceleration is due to the liquid-like property by the multiple charges.

Chapter 2. Experimental Procedure

2.1. HWCVD system

Figure 11 is a schematic diagram of HWCVD using in this study. The size of reaction chamber is 45 cm width and 40 cm length, respectively. A showerhead is placed upper side of chamber, and its diameter is 22 cm. Three tungsten filaments were used as hot wires and resistively heated using a DC power supply. The temperature of filaments was measured by an infrared optical pyrometer (RAYMR1SCCF, Raytek, USA).

Under the filaments, a shutter is placed for preventing substrate from being deposited before the deposition of SiC as Figures 11 and 12. It was located 1 cm above a substrate and its size is 15×15 cm^2, which is sufficient to cover deposition area of 1×1 cm^2 of a substrate. It was tested that nothing was deposited on the substrate when the shutter was closed in the entire process for about an hour and a half.

In order to control the substrate temperature, the distance between the substrate and the filaments was adjusted. The distance between filaments and a substrate was controlled from 8 mm to 20 mm by vertically moving substrate holder made of stainless steel.

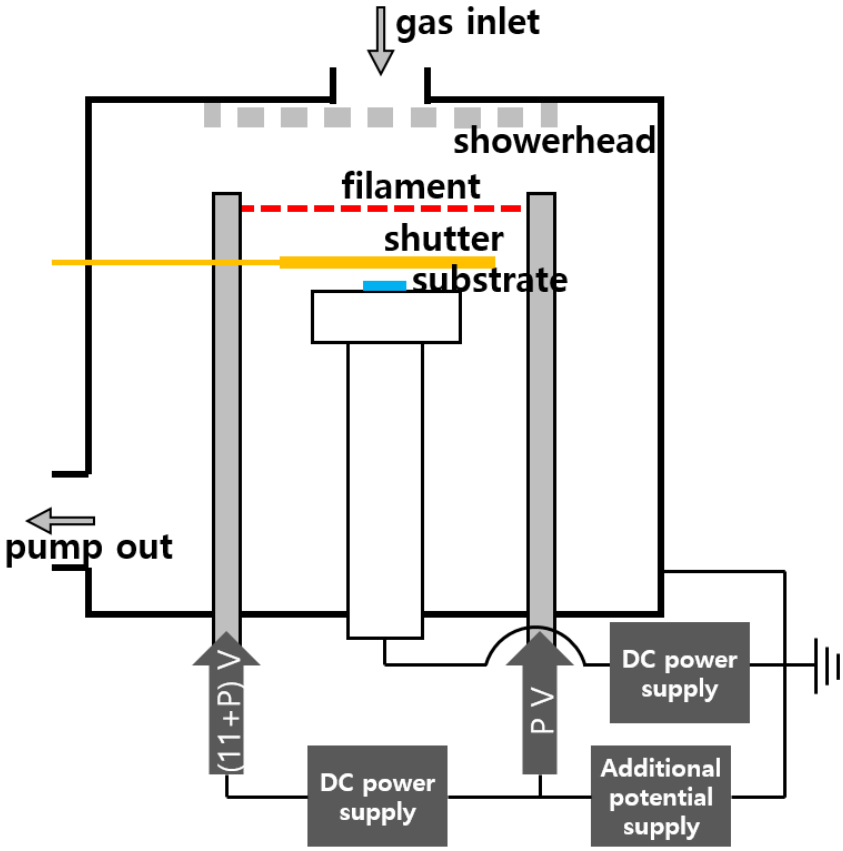

Figure 11. Schematics of HWCVD system.

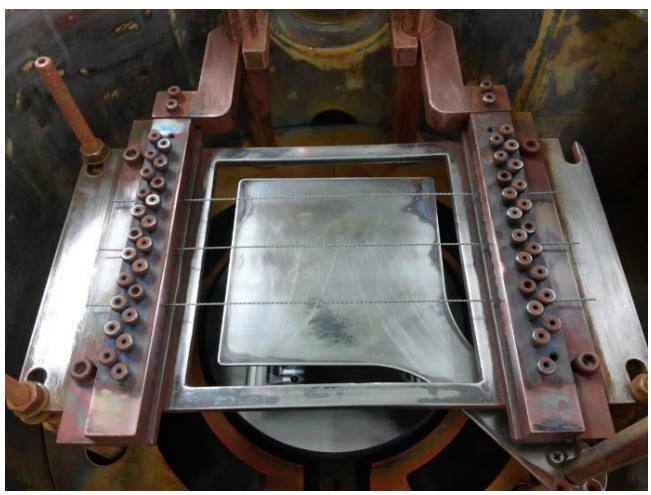

Figure 12. Filaments heating component and the shutter.

Pure silane (SiH_4, 99.9999%) and pure methane (CH_4, 99.9999%) were used as reactant gases. Pure hydrogen (H_2, 99.9999%) was used carrier gas. Gas flow were controlled by a mass flow controller (MFC, Tylan, USA). During the process, a baratron gauge (626A12TBE, MKS, USA) measured and monitored the reactor chamber pressure, and keep the pressure 1 torr by a pressure controller (651C, MKS, USA) equipped with a throttle valve.

A DC electric bias supply was connected to the substrate holder to create an electric field between the filaments and a substrate as shown in Figure 11. Above + 15 V or below – 200 V, DC glow charged occurred when filaments were heated at 2300°C.

Another DC electric bias supply was connected between the filament heating components and the ground to supply additional potential bias to the filaments as shown in Figure 11. When additional bias was P V, the potential difference between the end sides of a filament was (11+P) V at 2300℃. The additional bias was varied from + 50 V to – 50 V.

2.2. Procedure for capturing SiC nanoparticles

Before capturing of nanoparticles, a TEM grid with silicon monoxide (SiO) membrane on Cu mesh grid (Ted Pella, Inc., USA) was located on the substrate holder which was 8 cm below the filaments.

The following steps were taken before the capturing:

1. Three tungsten filaments were heated to 1400℃ for 10 min with 100 standard cubic centimeters per minute (sccm) of H_2 to removing organic substances or impurities on the surface of filaments.
2. Filaments were heated to 2100℃ with 4 sccm of CH_4 and 100 sccm of H_2 for carbonization for 10 min.
3. Filaments temperature and CH_4 flow rate were controlled to capturing temperature and flow rate, respectively.

In the process as above, the shutter remained closed until SiH_4 supplied. Then, while supplying SiH_4, the shutter was opened, and the substrate holder was raised to 2 cm below the filaments.

After capturing nanoparticles on the TEM grid for 30 sec, SiH_4 and CH_4 were turned off, the holder was lowered, and the shutter was closed.

2.3. Procedure for SiC films Growth

A 1×1 cm^2 diced 4H-SiC from a commercial 4 degree off, n-type, Si-faced, 4H-SiC wafer (Cree, Inc., USA) was used as a substrate. Substrates were prepared for cleaning steps by dipping in 10% hydrofluoric acid (HF) for 1 min and rinsing in deionized water.

The prior steps described in Chapter 2.2 were performed after a substrate was placed on the substrate holder. In that steps, the shutter remained closed as capturing process. Then the shutter was opened with supplying SiH_4 and substrate was raised to 2 or 8 mm below the filaments.

After 30 min of SiC film deposition, SiH_4 and CH_4 were turned off, the holder was lowered, and the shutter was closed. After turning off the H_2 and DC bias applied to the filaments to lower the temperature of the filaments, the sample was cooled while maintaining the chamber at base pressure.

2.4. Characterization

Raman spectroscopy was used for analyzing the crystallinity of films. Raman spectra were recorded with LabRam HR Evolution and LabRam Aramis (HORIBA, Japan) spectrometer. The 532 nm line of a diode pumped solid state (DPSS) laser and 514.5 nm line of an Ar-ion laser were used as the excitation source of LabRam HR Evolution and LabRam Aramis, respectively. The Raman excitation beam spot size is about 1 μm diameter. The Raman scattered light signal was collected in a backscattering geometry using the ×100 microscope objective lens.

SiC nanoparticles and films were observed for size measurement and crystallographic analysis by HRTEM using JEM-2100F (JEOL Ltd., Japan) and Tecnai F20 (FEI Company, USA). Using a field emission gun with an acceleration voltage of 200 kV, HR images, diffraction pattern (DP) images and scanning TEM (STEM) images were obtained.

HR images and DP images were analyzed using DigitalMicrograph (Gatan, Inc., USA) and STEM images were analyzed using ES Vision (FEI Company, USA).

Chapter 3. Generation of Charged SiC Nanoparticles during HWCVD

3.1. Introduction and Methods

Generation of CNPs in the gas phase during HWCVD processes was experimentally confirmed by Lee et al. [20] and Hong et al. [21, 22] in silicon deposition, and Jeon et al. [23, 24] and Park et al. [25] in diamond deposition as mentioned in Chapter 1.1.

Hong et al. [21] showed generation of CNPs during silicon HWCVD process with *in-situ* measurements using particles beam mass spectroscopy (PBMS), which can be used for measuring a size distribution of nanoparticles at low pressure. Figure 13 shows the size distribution of CNPs with various wire temperatures with a flowing gas mixture of 5%SiH_4–95%H_2 under 1.5 torr. Both positively and negatively charged silicon nanoparticles were generated in the HWCVD reactor, and as the temperature of hot wires increases, the size and the number of CNPs tends to decrease.

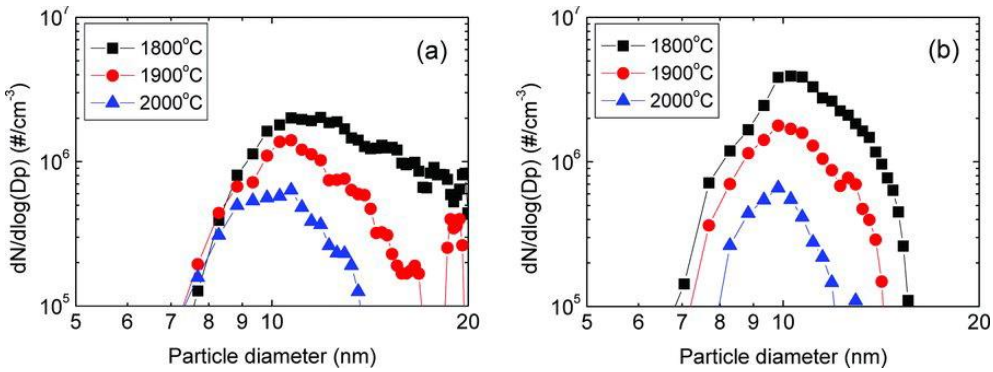

Figure 13. The size distribution of (a) positively and (b) negatively charged Si nanoparticles generated in the gas phase at various wire temperatures. By courtesy of Hong et al. [21].

Figure 14 shows STEM images of captured nanoparticles on a SiO membrane of a TEM grid at 600℃. Park et al. [25] confirmed the diamond nanoparticles generation in the hot filament CVD (HFCVD). The experiments condition was 3%CH_4-97%H_2, 2000℃ of filament temperature, and 20 torr. The lattice of nanoparticles observed by HRTEM corresponded to the diamond (111) plane. By capturing nanoparticles under different electric biases of + 75, 0, − 75, and – 200 V, the number concentration was decreased with increasing of the magnitude of the negative bias. These results indicate the nanoparticles are negatively charged during the diamond HFCVD process.

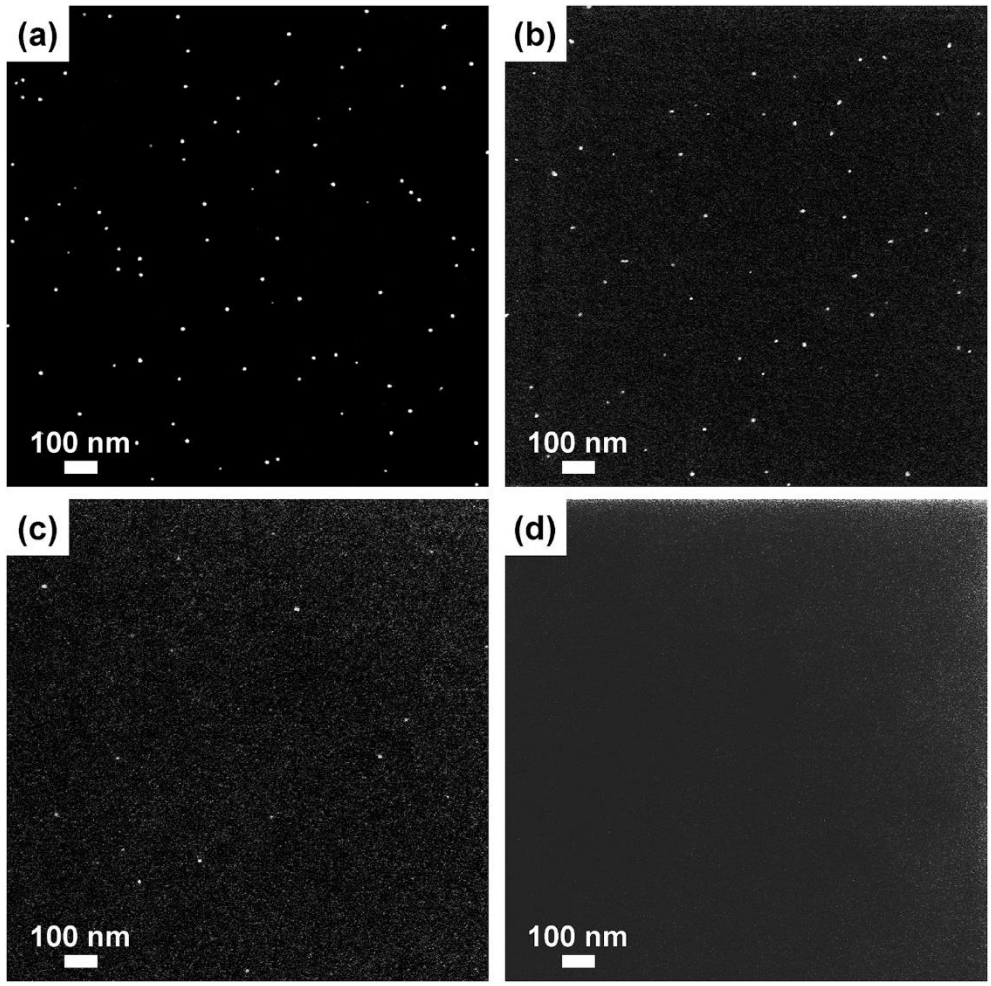

Figure 14. STEM images of diamond nanoparticles captured on TEM grid SiO membrane for 10 s under electric biases of (a) +75 V, (b) 0 V, (c) −75 V and (d) −200 V. By courtesy of Park et al. [25].

Hong et al. and Park et al. confirmed the presence of nanoparticles in the gas phase by applying electric biases using the charging properties of CNPs. In this study, it was observed that how nanoparticles behavior change with the process time to confirm that they are generated in the gas phase of

HWCVD. It can be argued that the SiC nanoparticles on the SiO membrane should not be captured from the gas phase but form directly on the SiO membrane by heterogeneous nucleation. If SiC nanoparticles are generated, they would grow in the gas phase with processing time. In this case, depending on whether they are captured in the initial or later stage of HWCVD, their size would be small or large. This means that if they are captured at different processing time, their size would be different. Using this method, Chung et al. [74] found out that the size of Si nanoparticles captured on the carbon membrane increased with processing time, which indicates that Si nanoparticles were generated in the gas phase. Similarly, here we tried to capture SiC nanoparticles at different processing time. For this, we introduce a new process parameter called a delay time. Normally, nanoparticles are captured and films are deposited in a scheme shown in Figure 15(a), where capturing or deposition starts immediately after precursor gases are supplied. When the delay time was used, capturing or deposition does not occur for the given delay time by closing the shutter. Capturing of nanoparticles or film deposition begins after the shutter is opened after the given delay time as illustrated by the scheme shown in Figure 15(b). In this way, SiC nanoparticles were captured for 30 sec with an increase in delay time from 0 sec to 5, 15, 30 and 60 min.

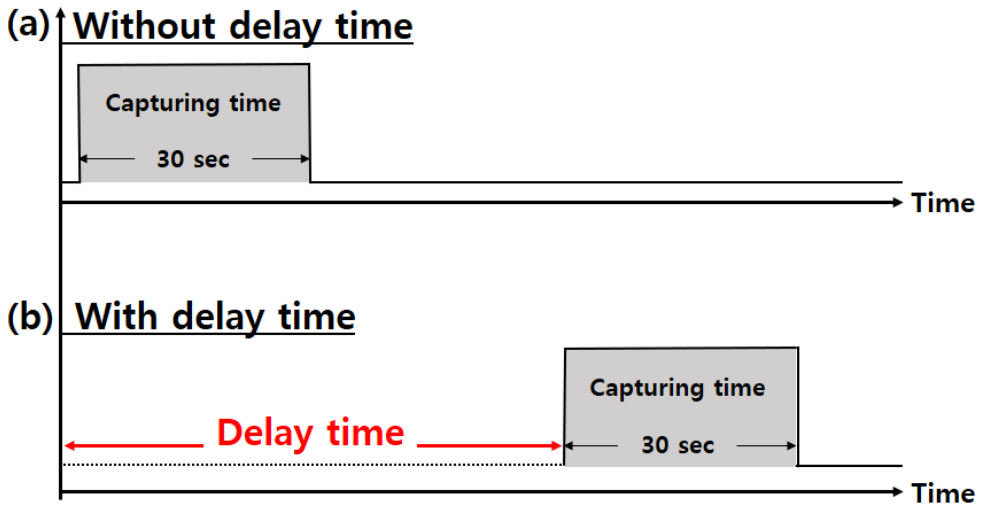

Figure 15. Schematics (a) without and (b) with delay time.

3.2. Result and Discussion

Figure 16 shows HRTEM and fast Fourier transform (FFT) images of SiC nanoparticles captured for 30 sec on SiO membranes of the TEM grid with delay times of 0, 5, 15, 30 and 60 min. The size of nanoparticles continued to increase with increasing delay time up to 60 min, which shows the effect of delay time. It was confirmed that when the shutter is closed during the delay time, no nanoparticles are captured on the TEM membrane. The average size was estimated from at least 30 SiC nanoparticles. In the absence or 0 min of delay time, the average size of SiC nanoparticles was 2.9 nm. The average size of captured SiC nanoparticles increased to 3.4, 4.1, 5.5 and 6.1 nm

respectively with increasing delay time of 5, 15, 30, and 60 min. SiC nanoparticles captured for the delay time of 0, 5, 15, 30 and 60 min are respectively shown in Figures 16(a)-(e). From the FFT images all nanoparticles were identified as SiC.

If these nanoparticles on the SiO membrane were not generated in the gas phase but nucleated and grew directly on the surface of the membrane by individual atomic or molecular units, their size should not change with the delay time because the capturing time of 30 sec was the same. Considering that the size of nanoparticles captured for 30 sec increased with increasing delay time as shown in Figure 16, it can be said that the SiC nanoparticles were generated in the gas phase.

Also, based on this result, it can be considered that charged nanoparticles generated during the process increase in size throughout the deposition processes. As will be mentioned later, size of charged nanoparticles is one of the main factors affecting the crystallinity of thin films. The smaller the size, the higher the probability of epitaxial growth on a crystalline substrate, so crystallinity control using the delay time may be possible.

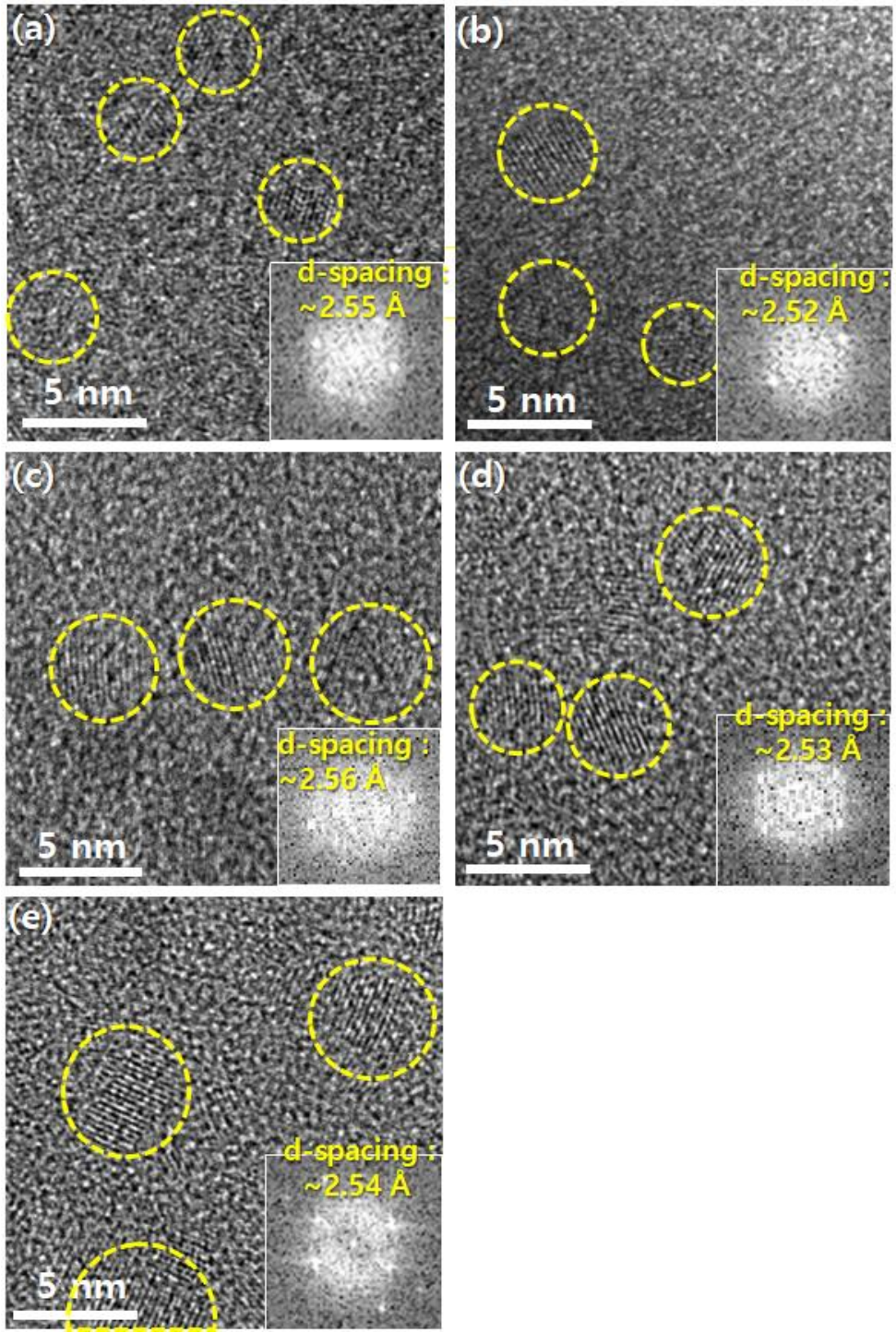

Figure 16. HRTEM and FFT images of SiC nanoparticles captured on a SiO membrane of a TEM grid for 30 sec with delay times of (a) 0, (b) 5, (c) 15, (d) 30 and (e) 60 min.

Considering that the flux of SiC nanoparticles generated in the gas phase is conserved, their number density is expected to decrease with the delay time. However, the number density of SiC nanoparticles with a delay time of 0, 5, 15, 30 and 60 min was 59, 61, 72, 78 and 72 per area of 100×100 nm2, respectively. When the delay time was short, the number density increases but after 15 minutes there is no significant difference.

Two possibilities could be considered for this. One is that if nanoparticles are charged, whose possibility would be examined later in this study, they are liquid-like if their size is small enough. In this case, they adopt the structure of the amorphous membrane on which they land. Then, they are not visible and cannot be resolved by TEM. The other is that if nanoparticles are charged, they can have Coulomb repulsion from the membrane and small nanoparticles have a smaller probability to land on the membrane than large ones.

3.3. Conclusion

TEM observation of SiC nanoparticles on the SiO membrane of the TEM grid

shows that the size of nanoparticles increased with delay time. Considering them, it can be said that the SiC nanoparticles are generated in the gas phase in the HWCVD process.

Chapter 4. Effect of Charge on the Behavior of Growth of SiC Films

4.1. Introduction and Methods

According to the detailed study of nanoparticles generated in the gas phase of the silicon and diamond HWCVD [12, 14], these nanoparticles are electrically charged. Song et al. [15] measured the negative current of 6–21 μA/cm^2 on the substrate during Si HWCVD process. This is a large amount that cannot be explained by the hot electron emission from the hot filament. Also, since not only negative current but also positive current was measured, it couldn't be explained only by the emission of hot electron.

When a metal filament of a high work function (WF) is heated to a high temperature, a large amount of electrons are released, which is called thermionic emission. The emission current density (J) is expressed by the Richardson-Dushman equation as follows in Equation (2 [16].

$$J_e = AT^2 \exp\left(-\frac{e\varphi}{kT}\right) = AT^2 \exp\left(-\frac{WF}{kT}\right) \quad (2)$$

J is the emission current density (A/m^2), A is the Richardson constant, T is a temperature of a metal in absolute temperature (K), k is Boltzmann constant (1.38×10^{-23} J·K^{-1}) and WF($e\varphi$) are work function of a metal (J).

Filaments used in HWCVD is heated to a high temperature of 1200℃ or higher for the decomposition of reactant gases. Tungsten or tantalum is used

as a raw material for filaments, and the work function of them is 4.5 eV and 4.21 eV, respectively, and have relatively low values among metals. Therefore, as shown in Equation (2, when the temperature of a metal increases, the metal with a low work function emits a large amount of electrons.

Applying an external electric field to a metal, the measured current value increases with increasing the magnitude of the electric field. This can be explained by Schottky effect or field enhanced thermionic emission, and is expressed by the following equation.

$$\Delta\varphi = \sqrt{\frac{e^3 E}{4\pi\varepsilon_0}} \tag{3}$$

E is magnitude of electric field, ε_0 is the vacuum permittivity. As shown in Equation (3, the electric field has effect of lowering the ionization energy barrier of the atom or molecule. That is, the stronger the external field applied to the filament, the greater the amount of electron emission from the surface. Considering this, Equation (2 could be modified as follows.

$$J_e = AT^2 \exp\left[-\frac{e}{kT}\left(\varphi + \sqrt{\frac{e^3 E}{4\pi\varepsilon_0}}\right)\right] \tag{4}$$

Reactant gases decomposed by hot filaments create atoms, molecules,

radicals, and nanoparticles. If the nanoparticles are adsorbed on the surface of the metal and remain for a sufficient time to reach the thermodynamic equilibrium, electron transfer between the metal and the adsorbed particles is possible. This will ionize the particles to give a positive or negative charge, and if the temperature of the metal surface is high enough to evaporate the nanoparticles, the ionized nanoparticles will evaporate into the gas phase. It has been suggested by Hwang and his colleagues [10, 17] that a nanoparticles can take or lose electrons from a metal by the difference between the work function of the metal and the work function of the nanoparticles through this series of steps.

The positively and negatively charged nanoparticles can be explained as follows. Equations 5 and 6 below represent Saha-Langmuir equation and the surface ionization of positive and negative particles, respectively.

$$\frac{n^+}{n^0} = \frac{g^+}{g^0} \exp\left(-\frac{\emptyset - WF}{kT}\right) \tag{7}$$

$$\frac{n^-}{n^0} = \frac{g^-}{g^0} \exp\left(-\frac{WF - E^i}{kT}\right) \tag{8}$$

n^0 is the number of neutral atoms of molecules that have evaporated without being ionized in contact with a metal. n^+ and n^- represent the number of positively or natively charged atoms or molecules, respectively. g^0, g^+ and g^- denote the statistical weight of neutral,

positively and negatively charged atoms or molecules, respectively. The ratio of these (g^+/g^0 or g^-/g^+) is nearly 1.

$\emptyset$ and E^i represent the ionization energy and electron affinity of the atom or molecule, respectively. According to this equation, when a gas atom or molecule having a low ionization energy contacts the surface of the hot filament, the gas is easily positively charged because the activation energy required to be positively charged is reduced by the size of the work function of the filament. Conversely, if a gas atom or molecule has a large electron affinity, it is more easily negatively charged when in contact with the thermal filament.

It was experimentally verified to confirm whether the SiC nanoparticles shown in Figure 16 occurs even during SiC film deposition in HWCVD. If they are charged, the capturing behavior of nanoparticles or the deposition behavior of films would be affected by the bias applied to the substrate. To check this possibility, nanoparticles were captured for 30 sec with biases of + 15 V, 0 V and – 200 V applied to the substrate using the DC bias supply shown in Figure 11 without any delay time.

In addition, SiC films were deposited for 30 min by applying biases of + 15 V, 0 V and – 200 V. When the bias voltage is above + 15 V or below – 200 V, DC glow discharge occurred between the substrate and the hot wires. When DC glow discharge occurred, unwanted porous dust was formed on the

substrate. For this reason, biases between – 200 V and + 15 V were applied during film deposition.

4.2. Result and Discussion

Figure 17 is the HRTEM image of nanoparticles captured under the bias. The average size of SiC nanoparticles captured under the biases of + 15 V and – 200 V was slightly decreased, respectively being 2.8 nm and 2.9 nm, compared with 2.9 nm of nanoparticles captured without the bias.

On the other hand, when the bias of + 15 V was applied to the substrate, the number density of captured nanoparticles was 51 per area of 100×100 nm2, which was a little bit smaller than that 58 per area of 100×100 nm2 for the bias of – 200 V and 59 per area of 100×100 nm2 for the bias of 0 V. The behavior of nanoparticles captured under the bias did not show any noticeable difference in size and number density.

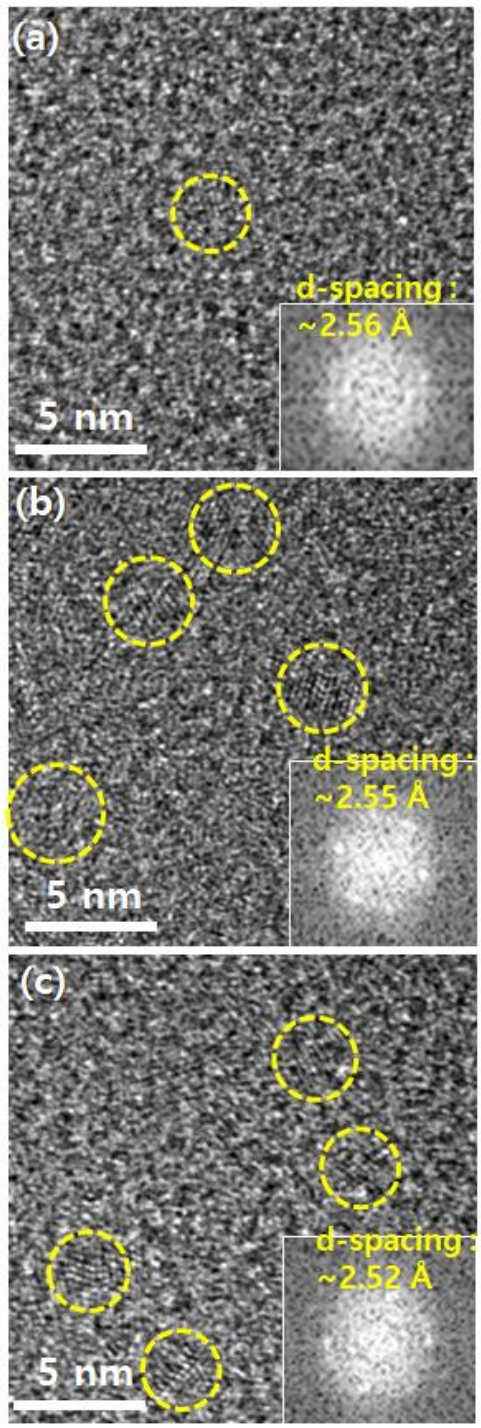

Figure 17. HRTEM and FFT images of SiC nanoparticles captured for 30 sec on SiO membranes of the TEM grid with substrate biases of (a) + 15 V, (b) 0 V and (c) – 200 V.

The deposition behavior of SiC thin films was also examined with the bias applied to the substrate. Figures 18(a)-(c) show low magnification TEM images and diffraction pattern (DP) of SiC films deposited, respectively, with substrate biases of + 15 V, 0 V and – 200 V. The SiC film deposited under 0 V was ~ 830 nm thick and it was ~ 760 nm under + 15 V, whereas the film deposited under – 200 V was ~ 430 nm thick. It should be noted that the film growth rate was decreased to half under the bias of – 200 V. The reduction of the film growth rate under the bias of – 200 V would be attributed to repelling the negatively charged flux, which indicates that an appreciable amount of depositing flux is negatively charged. Although it is expected that both positively charged and negatively charged nanoparticles are generated in the gas phase, the bias effect of – 200 V shown in Figure 17(c) indicates that the amount of negatively charged nanoparticles should be larger than that of a positively charged one.

In order to obtain the DP image, only the film area was selected using the selected area (SA) aperture so that the substrate area should be excluded from the DP image. The DPs in Figures 18(a) and 18b show that the films deposited under + 15 V and 0 V are polycrystalline. However, the DP in Figure 18(c) shows that the film deposited under – 200 V is single crystalline.

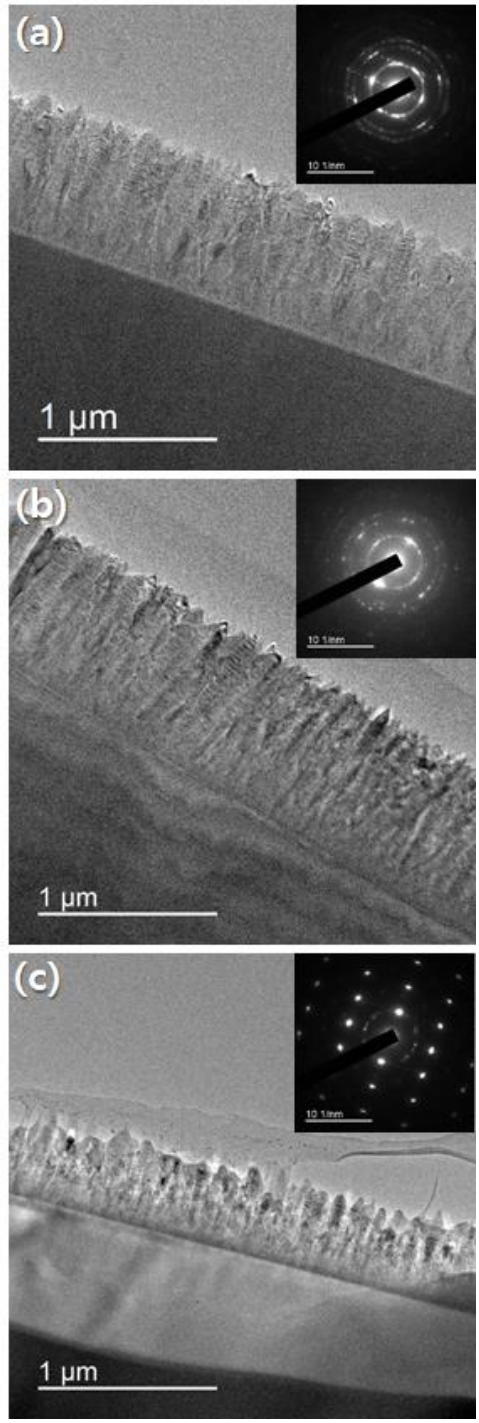

Figure 18. Low magnification TEM images of SiC films with substrate biases of (a) + 15 V, (b) 0 V and (c) – 200 V. Insets are diffraction pattern images in the deposited film.

HRTEM images of the films deposited under + 15 V, 0 V and – 200 V are shown respectively in Figures 19(a)-(c) and the magnified images of the box in Figures 19(a)-(c) are shown respectively in Figures 19(d)-(f). It is clearly revealed in Figures 19(d)-(f) that although the SiC films deposited under + 15 V and 0 V were polycrystalline, the film deposited under – 200 V was epitaxial up to the thickness of ~ 200 nm.

It is not clearly understood why the film of Figures 19(c) and 19(f) are epitaxial. One possible scenario that we can think based on our understanding of the deposition behavior of charged nanoparticles [12] is as follows. When – 200 V is applied to the substrate holder, initially positively charged nanoparticles would be attracted to the substrate and negatively charged nanoparticles would be repelled. Since SiC is insulating, positive charges would build up on the surface. These positive charges would not only reduce the bias effect of – 200 V but also repel the incoming positively charged nanoparticles. In the presence of such an electrostatic interaction, the incoming positively charged nanoparticles have difficulty in landing on the growing surface and would result in the low film growth rate of Figure 18(c). In such a situation, only those charged nanoparticles that can overcome the repelling electrostatic interaction would be allowed to land on the surface. Then, which nanoparticles can overcome the repulsive interaction?

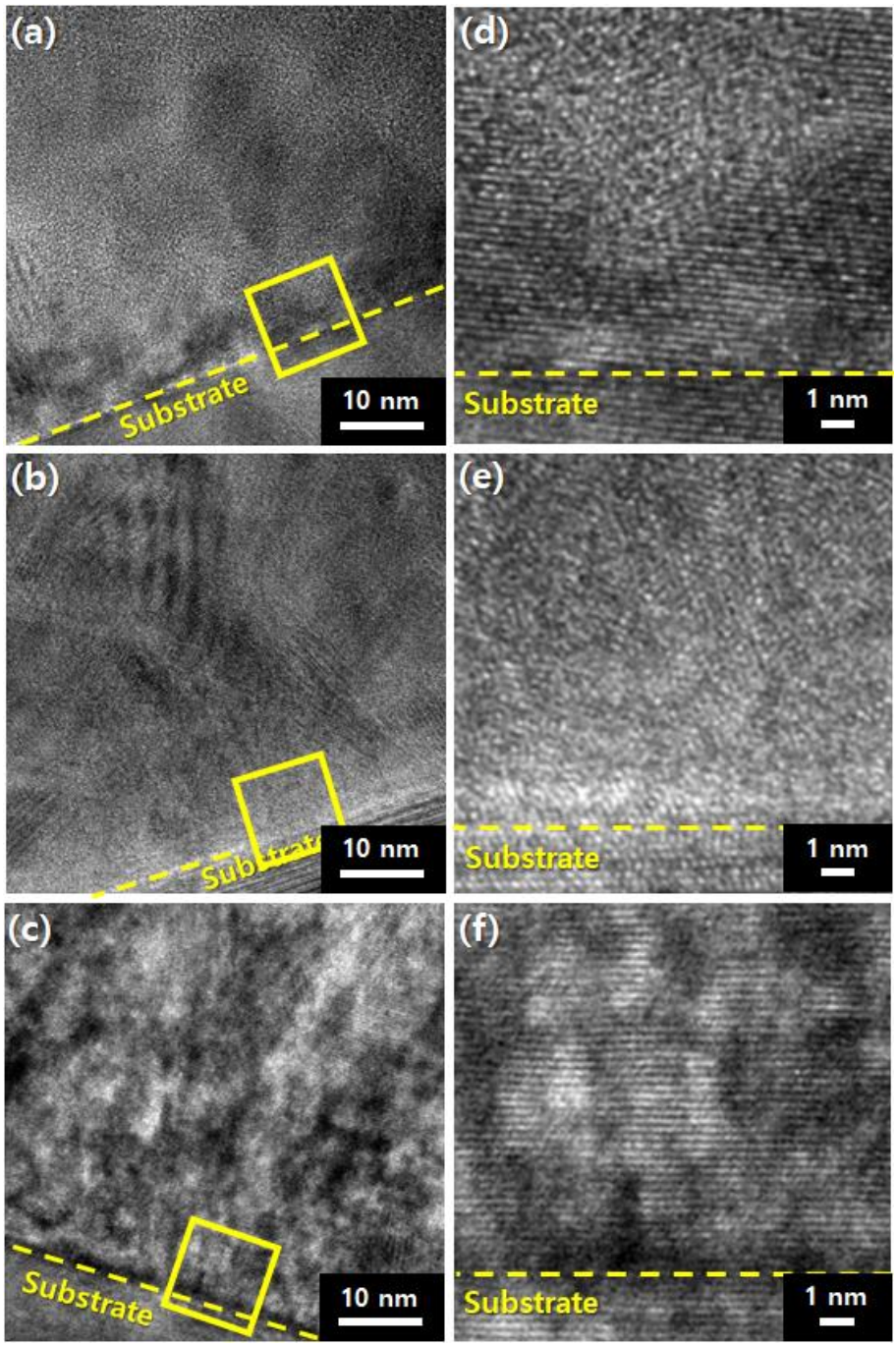

Figure 19. Cross-section HRTEM images of SiC thin films with substrate biases of (a) +15 V, (b) 0 V and (c) – 200 V. (d), (e) and (f) are enlarged images of interfaces of SiC films and substrates corresponding to the parts highlighted by the square in (a), (b) and (c), respectively.

Those would be nanoparticles which have the highest van der Waals attraction. When SiC nanoparticles approach the SiC single crystal substrate, the van der Waals attraction would depend on the misorientation between the nanoparticles and the substrate especially when they are close enough. When the attraction depends on the misorientation of nanoparticles with respect to that of the substrate, the incoming nanoparticles would rotate into such a misorientation to minimize the interaction energy. This misorientation would have an epitaxial relation with that of the growing surface. In other words, when nanoparticles rotate into an epitaxial orientation with the growing surface, the van der Waals attraction would be highest. These nanoparticles would overcome the repulsive electrostatic interaction on the growing surface and deposit epitaxially.

Figure 20 shows the cross-section HRTEM images of a film applied negative bias of – 200 V to substrate. Then, why did the epitaxial film change to a polycrystalline film after the film grew as thick as ~200 nm? The answer to this question would be the size increase of nanoparticles with the deposition time as shown in Figure 16, where the size of SiC nanoparticles increased with increasing delay time up to 60 min. According to the previous study on the deposition behavior of charged nanoparticles, small charged nanoparticles tend to be liquid-like, which favors epitaxial growth on the single crystalline substrate, losing their morphological and orientational identity.

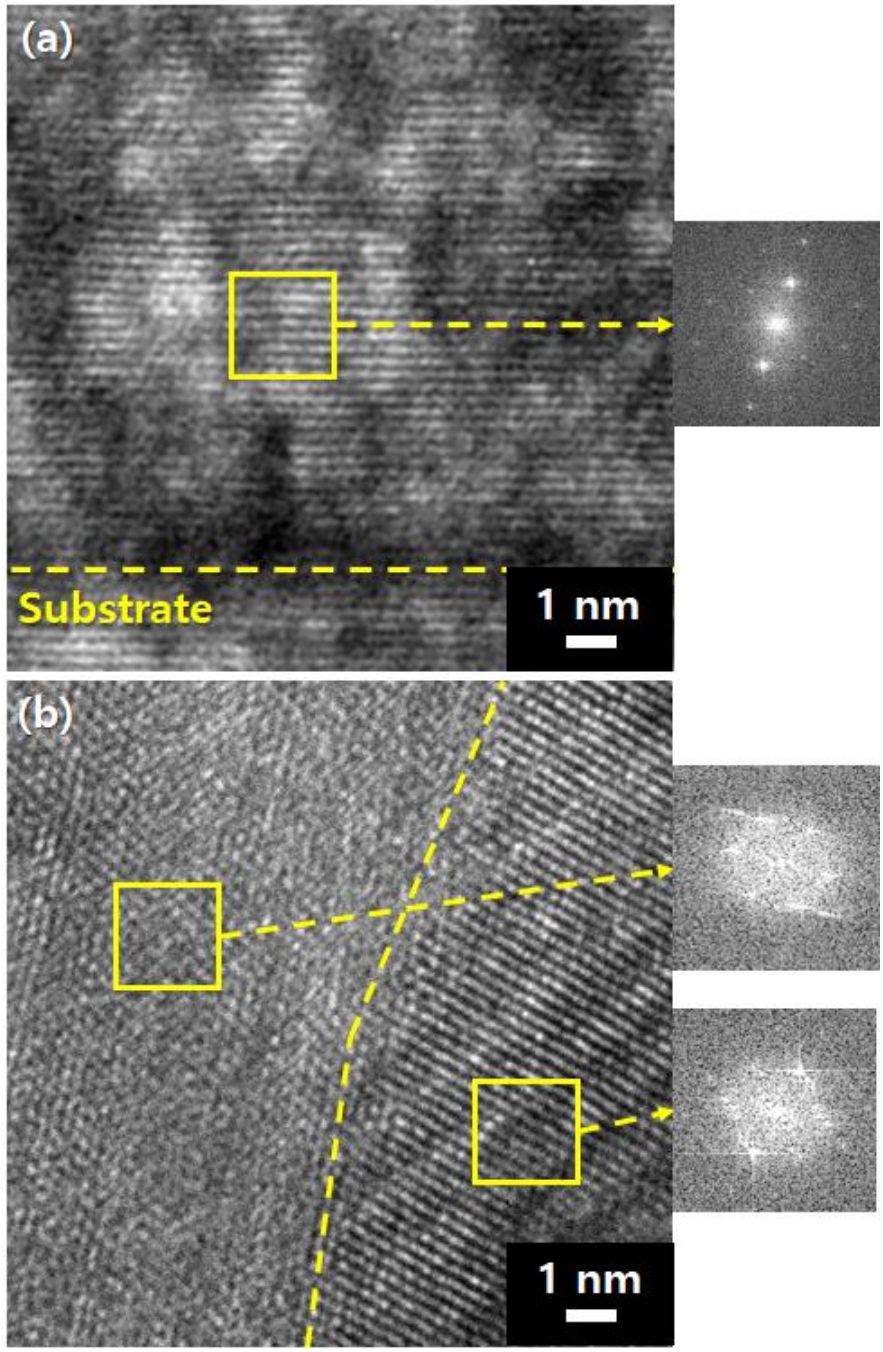

Figure 20. Cross-section HRTEM images of SiC film with a substrate bias of – 200 V of (a) the bottom and (b) middle regions. The insets on the right, indicated by arrows, are FFT images in the area.

Therefore, it is difficult to tell whether the film grew by individual atoms or nanoparticles. However, large charged nanoparticles tend to lose the liquid-like property and deposit as nanoparticles maintaining their morphological and orientational identity, producing a polycrystalline structure. This would be why the polycrystalline film was deposited near the top of the film shown in Figures 19(c) and (f).

4.3. Conclusion

The deposition behavior of SiC films was affected by the bias applied to the substrate, which indicates that nanoparticles should be charged. The homo-epitaxial film as thick as 200 nm could be grown by applying – 200 V to the substrate.

Chapter 5. Size Effect on Crystallinity of SiC Films

5.1. Introduction and Methods

Based on understanding of TCN, the amount of charge and size of nanoparticles are also important factor in film growth by CVD. According to this theory, the deposition behavior of nanoparticles changes drastically depending on whether nanoparticles are charged or neutral. Neutral nanoparticles tend to agglomerate randomly, producing a porous skeletal structure such as soot whereas CNPs tend to deposit as dense the deposition of dense films or nanostructures without voids as well as the epitaxial film growth by the building block of CNPs, Hwang [12] suggested that the presence of charge should make nanoparticles liquid-like especially when the size of nanoparticles is small enough.

In relation to the liquid-like property of CNPs, Iijima and his colleagues [61, 62, 75, 76] reported interesting observations that the shape of nanoparticles containing about 460 gold atoms itself constantly changed every few tenths of a second. The internal structure also changed from a single crystal to a twinned crystal and vice versa. With an increase of the nanoparticle size, the movement became slow and no rapid change was observed if it was larger than 100 Å. Most importantly, such dynamic evolution of the nanoparticles, which were active on insulating substrates such as SiO_2-covered Si and alumina, was slow and nanoparticles became sluggish when an electrically good conductor such as graphite or amorphous

carbon was used as a substrate [75]. Gold particles supported on a gold film remained inactive without undergoing translational motion or structural fluctuation [62].

The liquid-like property of CNPs appears to come from the combined effect of melting point depression of nanoparticles and the presence of charge. Therefore, the charge carried by nanoparticles plays an important role in non-classical crystallization [12]. One possibility for the role of charge would be to weaken the bond strength. In relation to this possibility, Clare et al. [60] studied the effect of charge on the bond strength of SiH_4 and Si_2H_6 by ab-initio calculations. They found out that the bond strength of Si-H in SiH_4 decreased from 3.9 eV to 0.98 eV and 0.30 eV, respectively, if SiH_4 is negatively and positively charged and the bond strength of Si-Si in Si_2H_6 decreased from 3.2 eV to 1.11 eV and 1.6 eV, respectively, if SiH_4 is negatively and positively charged.

The size of nanoparticles normally increases as the concentration of reactant gases increases. Experimentally it was confirmed that the size of nanoparticles influenced the deposition behavior of thin films and nanostructures. Jeon et al. [24, 77] showed that The size of gas phase nuclei was shown to increase with increasing methane concentration relative to hydrogen in the hot filament diamond CVD process. Figure 21 is mass distributions of negatively charged carbon nanoparticles with various CH_4 concentration. As mentioned before, small CNPs are more liquid-like than

large CNPs. Therefore, large CNPs measured under the high CH_4 concentration in Figure 21 would be less liquid-like and fail to accommodate their structure to the structure of a substrate. On the other hand, small CNPs measured under the low CH_4 concentration would be more liquid-like and grow with the structure of a substrate.

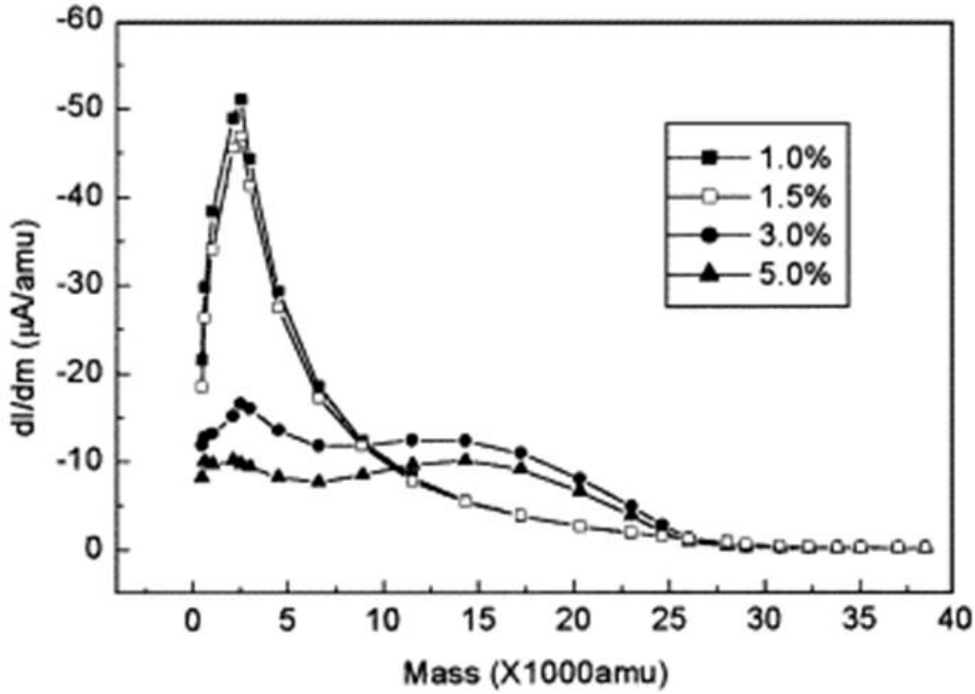

Figure 21. Mass distributions of negatively charged carbon clusters extracted from the hot filament reactor using gas mixtures of 1% CH_4–99% H_2, 1.5% CH_4–98.5% H_2, 3% CH_4–97% H_2, and 5% CH_4–95% H_2. By courtesy of Jeon et al. [77].

Since the gas phase nuclei are thought to have a diamond phase, diamond nanoparticles are synthesized automatically in the gas phase during the diamond CVD process. In order to obtain diamond nanoparticles, all we have to do is to capture them in a suitable way. They also showed that good quality diamonds were deposited by 1%CH_4–99%H_2 and ball-like diamonds called cauliflower structures were deposited by 3%CH_4–99%H_2.

Using the change in the liquid-like property with the size difference of the nanoparticles, Jung et al. [26] grown the homo-epitaxial silicon thin film in the silicon HWCVD process. They continuously supplied the small size of nanoparticles using cyclic process, which is to repeatedly perform the deposition process. Figure 22 shows cross-section images of silicon thin film deposited epitaxially using the cyclic process. This result shows that the size of nanoparticles is an important factor in controlling the crystallinity of the films by continuously supplying small CNPs on the crystalline substrate.

In order to confirm how the size of SiC nanoparticles changes with the process variables, SiC nanoparticles were captured under various process conditions.

First, to observe the size change of the nanoparticles with the filament temperature, the temperature of filaments was changed from 1800℃ to 2300℃, and nanoparticles were captured on a SiO membrane on Cu mesh TEM grid.

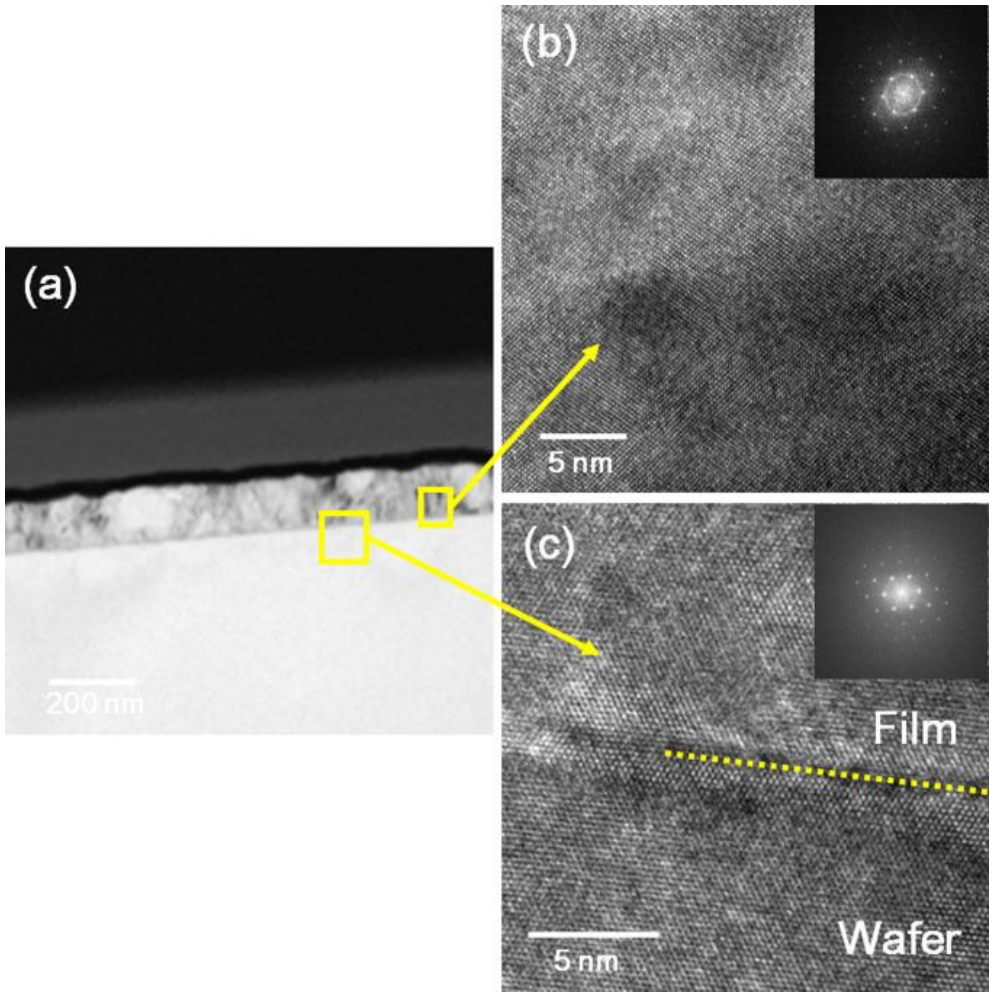

Figure 22. TEM cross section images of the silicon film deposited on (100) silicon wafer with 6 times of the cyclic deposition process for 30 sec (a) Low magnification TEM image of films, (b) HRTEM image of the upper gray layer, and (c) HRTEM image of the interfacial region between the silicon wafer and the film. By courtesy of Jung et al. [26].

Then effect of the concentration of the reactant gases on size of nanoparticles was confirmed by capturing nanoparticles on a SiO membrane on Cu mesh TEM grid with various ratio of reactant gases. The ratio of (SiH_4 + CH_4)/H_2 was varied from 0.04 to 0.01 for control the concentration of reactant gases. As previously mentioned, it could be predicted that the size of nanoparticles decreases with increasing concentration of reactant gases.

To confirm the effect of the electric bias applied to the hot wires, the additional potential supply was installed in the HWCVD system as shown in Figure 11. The additional potential supply for the bias is connected between the ground and the DC power supply for filaments. The DC voltage difference between the both sides of filaments was 11 V at the filament temperature of 2300℃. Therefore, the bias voltage is P, the potential difference between the ends of the wires is (11 + P) V at 2300℃. The additional bias could be varied from – 50 V to + 50 V. When the magnitude of bias is over 50 V, DC glow discharge occurred.

Nanoparticles were captured on SiO membrane on Cu mesh TEM grid with the additional filament biases for 30 sec. SiC nanoparticles captured on the Cu TEM grid were observed using TEM.

In addition, to confirm how the crystallinity of the films are affected by the size of the nanoparticles, SiC films were deposited under various conditions

to change the size of CNPs. SiC films deposited on the 4H-SiC substrate were observed using TEM and Raman Spectroscopy.

5.2. Result and Discussion

Figure 23 shows the TEM observation of the SiC nanoparticles captured on the SiO membrane of the Cu TEM grid at four different filaments temperatures. When the filaments temperature is 2300℃, SiC nanoparticles of 2 ~ 3 nm were captured. The size of SiC nanoparticles increased to 5 ~ 8 nm at the filaments temperature of 2000℃. Therefore, the size of the SiC nanoparticles increased with decreasing the filament temperature. This would be because collision between particles increases as the electron emission from surface of filaments decreases, which is described by the Richardson-Dushman equation [16], with decreasing the filament temperature. According to Richardson-Dushman equation, as temperature of filaments increases, thermionic emission of electrons increases. Then, probability that nanoparticles are negatively charged increases. Interaction between these single charged nanoparticles can be repulsive, and accordingly, the size of nanoparticles can be decreased.

In contrast, the number concentration of nanoparticles was not much affected by the filament temperature. On the other hand, when the temperature

was lowered to 1800℃, much larger Si nanoparticles instead of SiC nanoparticles were deposited. This would be because the temperature of the tungsten wire was not high enough to decompose all CH_4 supplied from the shower head. It should be noted that CH_4 is much more difficult to decompose than SiH_4.

In the HWCVD process, hot wires play an important role not only in decomposing precursor gases but also in charging nanoparticles through thermionic electron emission. Based on the TCN, if CNPs are small enough at the given temperature, they tend to have a liquid-like property and to undergo epitaxial recrystallization, which can produce epitaxial films. If CNPs are not small enough, they have difficulty in undergoing epitaxial recrystallization, producing twin or grain boundaries with the growing surface. Still, they produce a void-free dense structure of films. Therefore, small CNPs are favorable for the growth of epitaxial films whereas large CNPs are favorable for the growth of polystructured films.

Increasing the deposition temperature is another way to make CNPs liquid-like. If CNPs are liquid-like, they would accommodate their structure to that of the substrate, which is beneficial for epitaxial growth [12, 26, 78]. Therefore, increasing the wire temperature would be favorable for epitaxial growth. When the wire temperature was raised above 2300℃, however, tungsten tended to be evaporated from the wires, contaminating the films. Therefore, in the HWCVD process using tungsten wires, the wire temperature

should not be increased above 2300℃ [79].

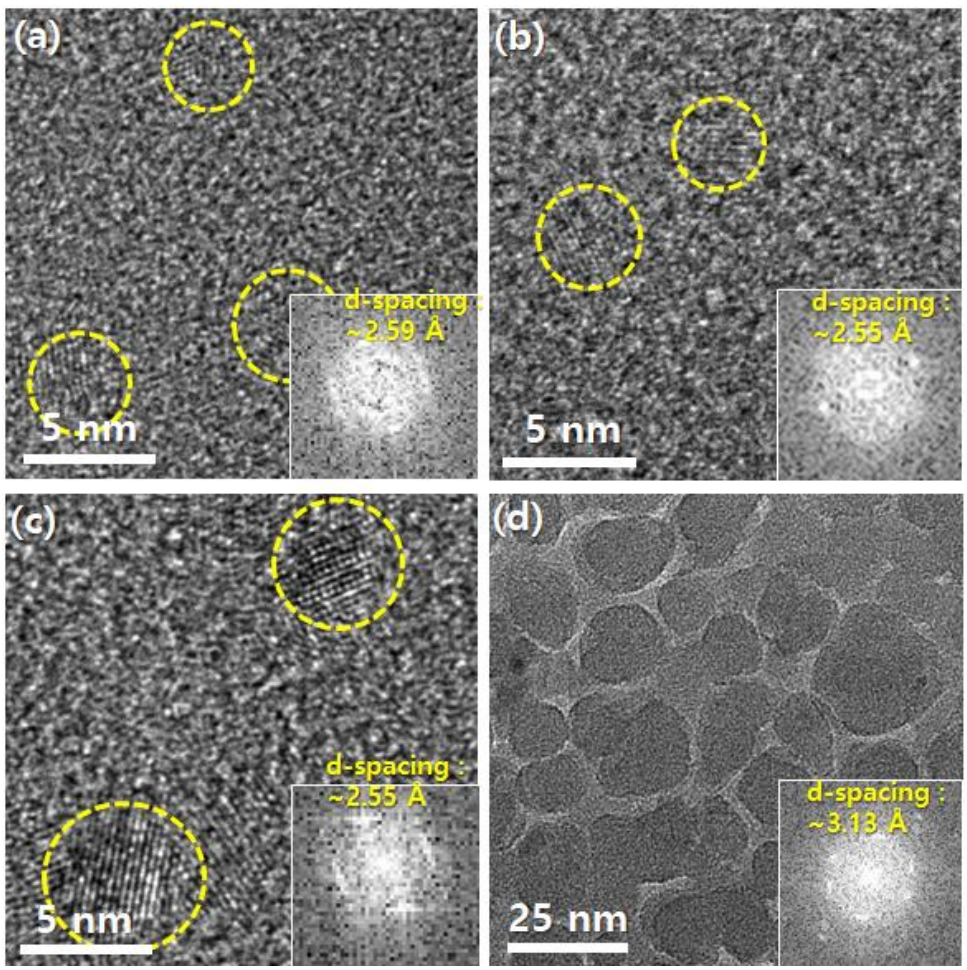

Figure 23. TEM images of SiC nanoparticles on TEM grids at filament temperatures of (a) 2300, (b) 2200, (c) 2000 and (d) 1800℃.

Figures 24(a)–(c) show TEM images of captured SiC nanoparticles with varying ratios of $(SiH_4 + CH_4)/H_2$ of 0.04, 0.02 and 0.01, respectively. Under all three conditions, SiC nanoparticles of 1 ~ 3 nm were captured. As to the size of the nanoparticles, there seems to be little difference with precursor concentrations. On the other hand, as the precursor concentration decreased, the number concentration of SiC nanoparticles also decreased. When the gas ratio of $(SiH_4 + CH_4)/H_2$ was 0.01, almost no nanoparticles were observed; only a few nanoparticles of 1 ~ 2 nm were observed. This is because amount of precipitation of SiC decreases as the concentration of precursor gases decreases, thereby reducing the size of nanoparticles.

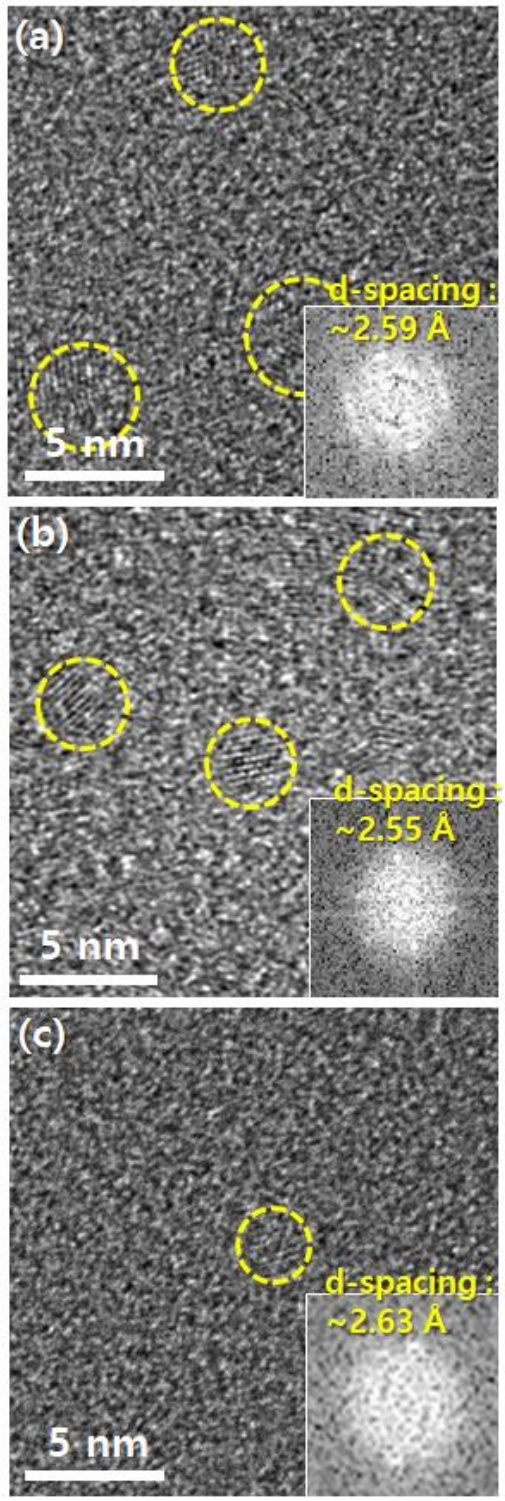

Figure 24. HRTEM images of SiC nanoparticles captured with the reactant gas ratio of $(SiH_4 + CH_4)/H_2$ of (a) 0.04, (b) 0.02 and (c) 0.01.

Park et al. [38] studied the electric field formed around the hot wires during Si HWCVD using a Maxwell software. They also measured the current near the input and output positions of the hot wires when the DC bias was applied to the hot wires. When the bias was + 25 V, the measured current was + 2.38 nA/cm^2 below 1.5 cm of the input position of the hot wires. When the bias of – 25 V was applied to the hot wires, however, it produced – 4.86 x 104 nA $/cm^2$ at the same position. This means that when the negative bias is applied to the hot wires, it could produce a much higher density of electrons or negatively-charged species, which can produce smaller CNPs.

About the property of nanoparticles, Fujita [39, 40] reported that if nanoparticles are below a certain size called magic size, their property such as diffusivity changes abruptly. For example, diffusivity increases so abruptly high below the magic size that small nanoparticles are almost liquid-like. Fujita suggested that the magic size for SiC is 3 ~ 5 nm. If Fujita's concept of magic size is combined with the theory of CNPs, small CNPs tend to be liquid-like and to accommodate their structure to that of the substrate. Considering such an abruptly high diffusivity below a magic size, the smallest CNPs would be favorable for epitaxial recrystallization at the given temperature. The smallest CNPs are expected when the gas ratio of (SiH_4 + CH_4)/H_2 was 0.01 and the bias of – 50 V was applied to the hot wires at the same time. In other words, when the gas ratio of (SiH_4 + CH_4)/H_2 was 0.01 with the bias of – 50 V applied to the wires, the size of CNPs would be so

small and thereby liquid-like that CNPs accommodate their structure to that of the SiO membrane.

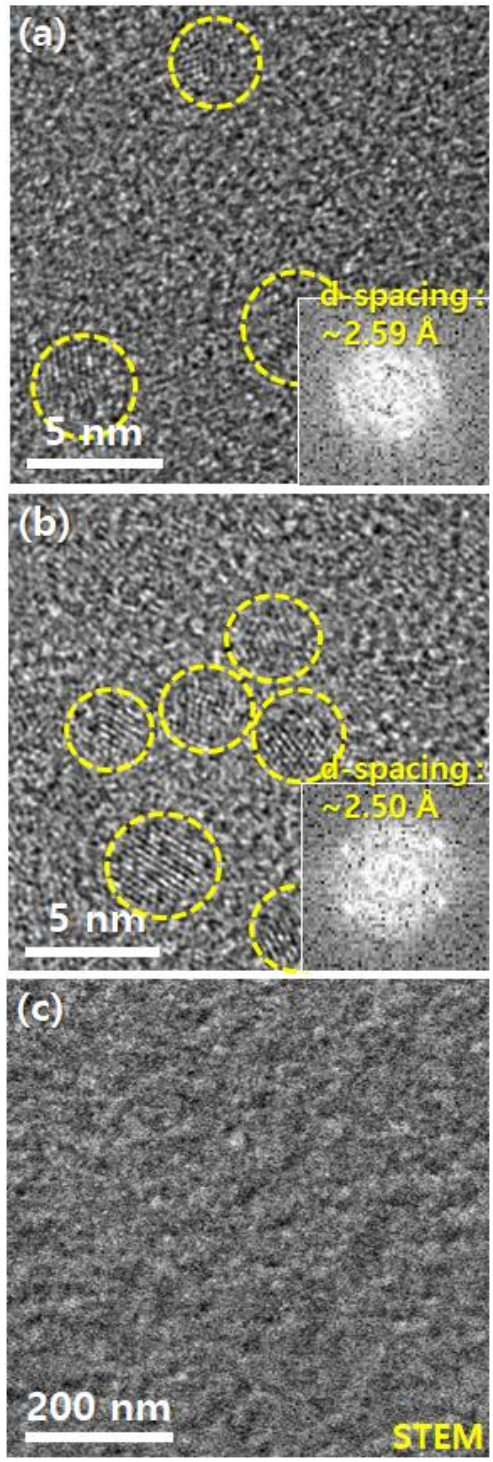

Figure 25. TEM and STEM images of SiC nanoparticles with additional hot wire biases of (a) 0 V, (b) + 50 V and (c) – 50 V.

Figure 26 shows the cross-section TEM image of SiC films deposited at the gas ratio of $(SiH_4 + CH_4)/H_2$ of 0.04 and 0.01 under the bias of – 50 V at the wire temperature of 2300°C. The TEM and the FFT images of Figure 26(a), which was deposited at the gas ratio of $(SiH_4 + CH_4)/H_2$ of 0.04, shows that a polycrystalline SiC film was grown. However, Those of Figure 26(b), which was deposited at the gas ratio of $(SiH_4 + CH_4)/H_2$ of 0.01, an epitaxial SiC film of ~ 30 nm was grown.

Figure 26 agrees with the hypothesis made by the theory of CNPs: small CNPs are liquid-like and favorable for epitaxial growth whereas large CNPs are less liquid-like and favorable for polystructure growth. According to the theory of CNPs, if the substrate temperature is increased, it would further favor the condition of epitaxial growth. To increase the substrate temperature, the distance between the hot wires and the substrate was reduced from 8 mm to 2 mm with the other conditions being the same as those of Figure 26(b). The result is shown in Figure 27, where an epitaxial SiC film of ~ 100 nm was grown.

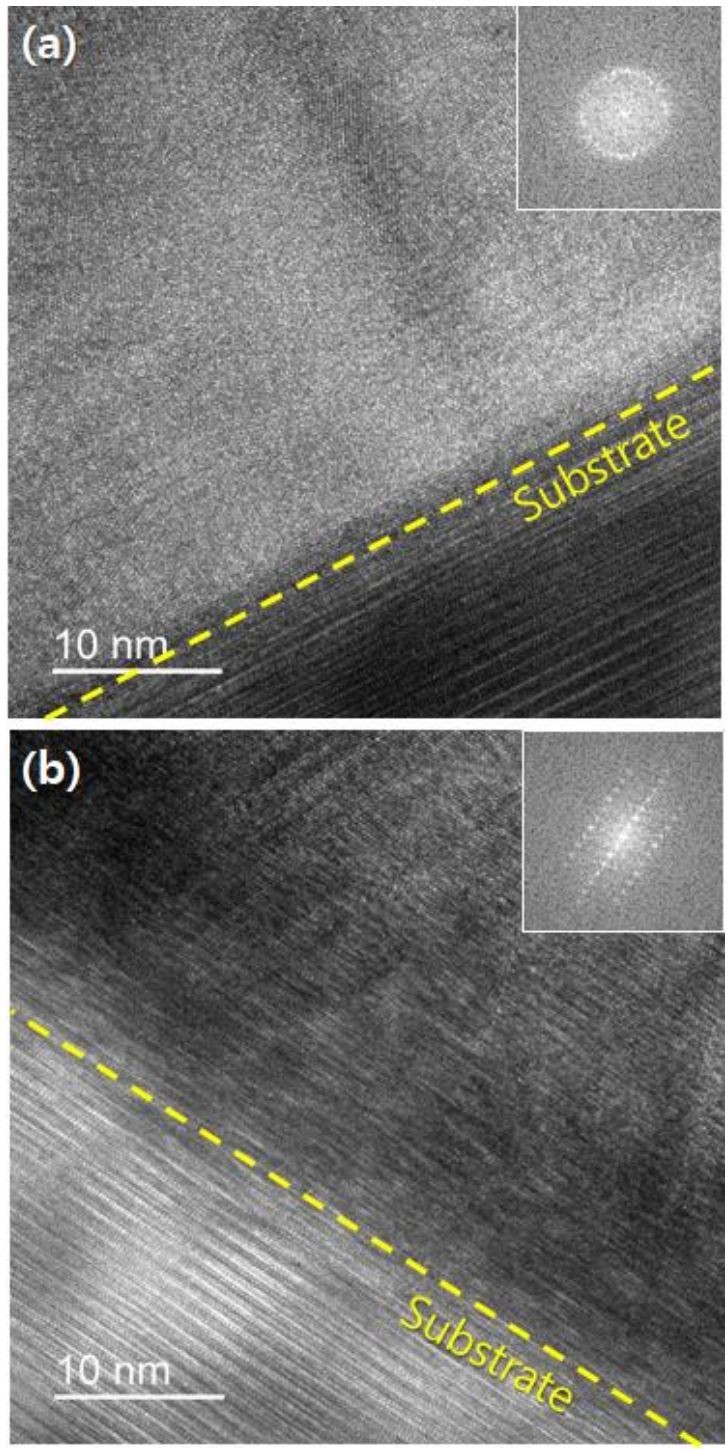

Figure 26. Cross-section TEM images and FFT images of SiC films deposited with an additional filament bias of – 50 V and he gas ratio of $(SiH_4 + CH_4)/H_2$ of (a) 0.04 and (b) 0.01.

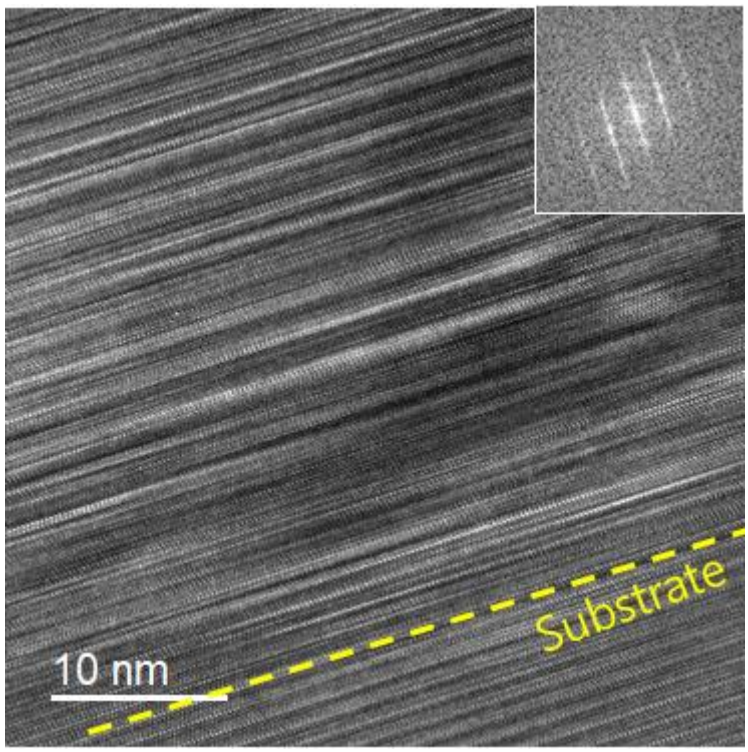

Figure 27. Cross-section TEM and FFT images of a SiC films deposited by the gas ratio of $(SiH_4 + CH_4)/H_2$ of 0.01, the wire bias of – 50 V, and the distance of 2 mm between the wires and the substrate.

Figure 28 shows the cross-section TEM images of the SiC film deposited under the gas ratio of $(SiH_4 + CH_4)/H_2$ of 0.01, the wire bias of – 50 V, and the distance of 2 mm between the filaments and the substrate. The epitaxial film changed to the polycrystalline film after the film grew as thick as ~ 100 nm like previously described in Chapter 4. The reason why the crystallinity of the film changed to polycrystalline also can be explained the increase of size of CNPs during the film deposition. Due to the size increase, growth of epitaxial thin films above a certain level becomes difficult.

‘

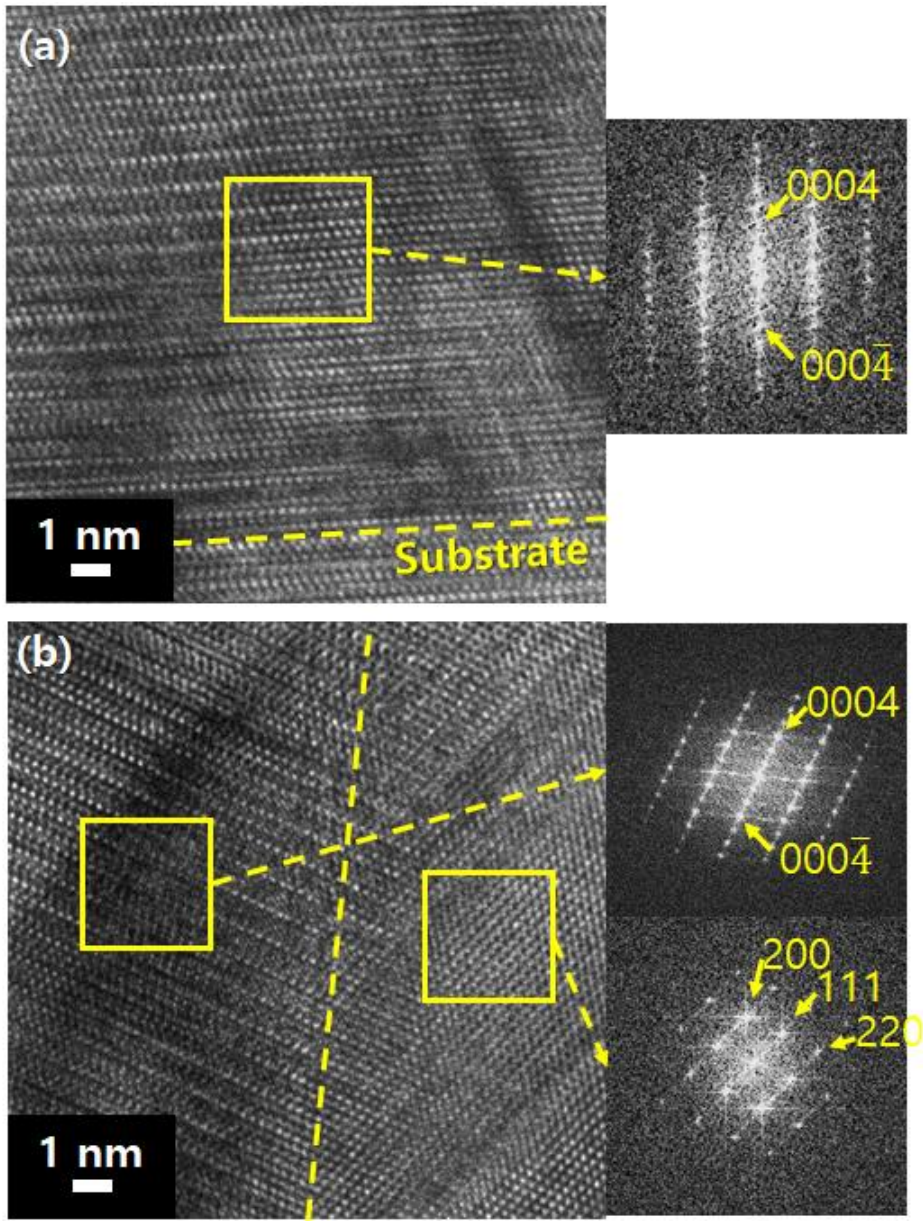

Figure 28. Cross-section HRTEM images of (a) the bottom and (b) the middle region of the SiC film in Figure 27. The insets on the right, indicated by arrows, are FFT images in the area.

Figure 29 shows the Raman spectra of SiC films deposited under various conditions. Figure 29(a) shows the data where the gas ratio of (SiH_4 + CH_4)/H_2 was 0.04 without applying the bias to the wires. Figure 29(b) shows the data where the gas ratio of (SiH_4 + CH_4)/H_2 was 0.04 with the bias +50 V applied to the wires. In both cases, an amorphous SiC (a-SiC) peak was observed in the low Raman shift region and a silicon peak was also observed at 520 cm^{-1}.

Figures 29(c)–(e) show the Raman spectra of SiC films with the bias of –50 V applied to the wires. The higher intensity of 4H-SiC transverse optical (TO) at 776 cm^{-1} of Raman shift corresponds to the higher crystallinity. In Figures 29(d) and (e), the gas ratio of (SiH_4 + CH_4)/H_2 was decreased to 0.01. The peak intensities for 4H-SiC TO at 776 cm^{-1} of Figures 29(d) and (e) are much higher than those of Figures 29(a)–(c). Comparing the peak intensity between Figures 29(d) and (e), reducing the distance between the wires and the substrate from 8 mm to 2 mm increases the crystalline quality.

Considering all the results of Figure 24–Figure 29, the size of CNPs is an important factor in determining the crystallinity of films. The substrate temperature is also an important factor.

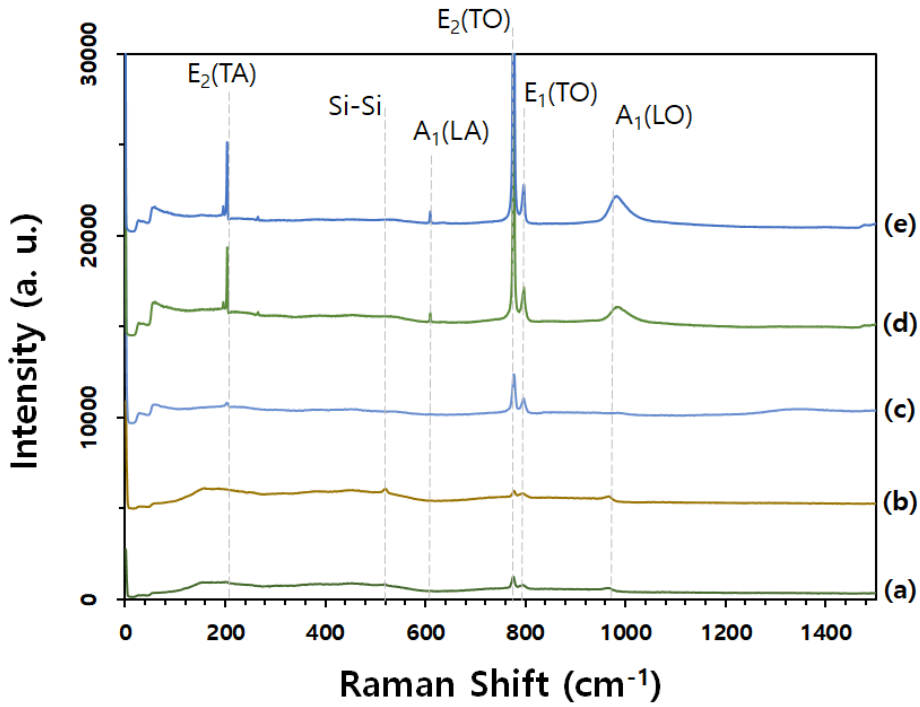

Figure 29. Raman spectra of the SiC films deposited at five different conditions: (a) without the bias and the gas ratio of (SiH_4 + CH_4)/H_2 of 0.04, (b) with the bias of + 50 V and the gas ratio of (SiH_4 + CH_4)/H_2 of 0.04, (c) with the bias of – 50 V and the gas ratio of (SiH_4 + CH_4)/H_2 of 0.04, (d) with the bias of – 50 V and the gas ratio of (SiH_4 + CH_4)/H_2 of 0.01, and (e) with the bias of – 50 V, the gas ratio of (SiH_4 + CH_4)/H_2 of 0.01 and the distance of 2 mm between the wires and the substrate.

5.3. Conclusion

The size of the SiC nanoparticles decreased with the filament temperature was increased, the concentration of the precursor was decreased, and a negative bias was applied to the hot wires during a SiC HWCVD process. It was found that an epitaxial SiC film could be grown under the condition that the SiC nanoparticles were small, which was achieved by decreasing the precursor concentration and applying the negative bias to the wires. Increasing the substrate temperature by reducing the distance between the wires and the substrate was also favorable to the growth of the epitaxial SiC film.

Summary

Silicon carbide has been extensively studied for candidates to replace the silicon as a wide band gap semiconductor. Crystallinity of SiC films deposited using a HWCVD reactor could be controlled by process variables such as filament temperature, substrate temperature and concentration of precursor gases and so on. In this study, microstructure control of SiC films studied using phenomenological evidences by controlling the behavior of SiC nanoparticles using characteristics of SiC nanoparticles generated in the gas phase of HWCVD based on the understanding of theory of charged nanoparticles.

Considering the size of SiC nanoparticles increased from 2.9 nm to 6.1 nm with increasing delay time, it could be said that the SiC nanoparticles were generated in the gas phase in the HWCVD process. In addition, it can also be considered that the size of nanoparticles generated in the gas phase increases throughout the film deposition processes.

According to the theory of charged nanoparticles, since these nanoparticles are charged, their deposition behavior is affected by the electric field. Thus, microstructure of SiC film was affected by the bias applied to the substrate. When a bias of – 200 V was applied to the substrate, an epitaxial SiC film of

about 200 nm was deposited. On the other hand, when no bias or positive bias was applied to the substrate, polycrystalline SiC films were deposited.

Small size of charged nanoparticles have liquid-like properties. They tends to accommodate their structure to the crystal structure of a substrate. When a substrate is crystalline, small size of nanoparticles grow epitaxially on substrate, whereas large size of nanoparticles grow non-epitaxially.

Nanoparticles captured on SiO membrane of Cu mesh TEM grid were observed after varying the filament temperature and the concentration of precursor. As the filament temperature reduced, the size of SiC nanoparticles increased. Silicon nanoparticles were observed with decreasing filament temperature due to the difference in decomposition between CH_4 and SiH_4. In addition, as the concentration of precursor decreased, the particles size and number concentration decreased.

SiC nanoparticles were captured and observed with different base potential of filaments. No nanoparticles was observed when negative bias was applied to the filaments, on the other hand, when the positive bias was applied to the filament, the number density and size of nanoparticles were similar to those when the additional bias was not applied. When the additional negative and positive biases were applied to the filament, the change in magnitude of current was large when a negative bias was applied. It could be thought that nanoparticles exist when a negative bias was applied to the filaments, because

the film was deposited under this condition, but they were small enough to accommodate their structure to amorphous structure of TEM grid.

Based on the understanding of theory of charged nanoparticles described above, thin films were deposited under various processes. From the Raman spectra, it was confirmed that the crystallinity of films was poor when no bias was applied or when a positive bias was applied to the filaments. The crystallinity of films deposited with additional filament bias of – 50 V was improved. This experimentally proved that the size of the SiC nanoparticles was decreased, and thus the crystallinity of SiC films was improved.

The crystallinity of SiC films was further improved by applying negative bias to the filaments and reducing the concentration of the precursor gases. It was confirmed by observation using TEM that a 30 nm thick homo-epitaxial SiC film was grown in the bottom region of the film. Raising the temperature of substrate would be helpful for improving the crystallinity of films, so the distance between the filaments and the substrate was closed to 2 mm under the same conditions. It was confirmed that SiC film was epitaxially grown as thick as about 100 nm in the bottom region of the film.

These results show that charged nanoparticles generate in the gas phase during SiC HWCVD process, and their diffusivity is enhanced with the charge. This means the size and charge of the nanoparticles can be important process parameters in deposition of SiC film.

Bibliography

1. Deblecker, O., Z. De Grève, and C. Versèle, *Comparative Study of Optimally Designed DC-DC Converters with SiC and Si Power Devices.* Advanced Silicon Carbide Devices and Processing, 2015: p. 143-173.

2. Millán, J., et al., *A survey of wide bandgap power semiconductor devices.* IEEE transactions on Power Electronics, 2013. **29**(5): p. 2155-2163.

3. Cheung, R., *Silicon carbide microelectromechanical systems for harsh environments*. 2006: World Scientific.

4. Codreanu, C., et al., *Comparison of 3C–SiC, 6H–SiC and 4H–SiC MESFETs performances.* Materials Science in Semiconductor Processing, 2000. **3**(1): p. 137-142.

5. Finger, F., et al., *Microcrystalline silicon carbide alloys prepared with HWCVD as highly transparent and conductive window layers for thin film solar cells.* Thin Solid Films, 2009. **517**(12): p. 3507-3512.

6. Tabata, A., et al., *Growth of silicon carbide thin films by hot-wire chemical vapor deposition from $SiH_4/CH_4/H_2$.* Thin Solid Films, 2009. **517**(12): p. 3516-3519.

7. Chen, T., et al., *Microstructure and electronic properties of microcrystalline silicon carbide thin films prepared by hot-wire CVD.* Thin Solid Films, 2011. **519**(14): p. 4511-4515.

8. Tehrani, F.S., et al., *Low-pressure synthesis and characterization of multiphase SiC by HWCVD using CH_4/SiH_4.* Vacuum, 2012. **86**(8): p. 1150-1154.

9. Pawbake, A., et al., *Growth of boron doped hydrogenated nanocrystalline cubic silicon carbide (3C-SiC) films by Hot Wire-CVD.* Materials Research Bulletin, 2016. **76**: p. 205-215.

10. Hwang, N.-M. and D.-Y. Kim, *Charged clusters in thin film growth.* International Materials Reviews, 2004. **49**(3-4): p. 171-190.

11. Hwang, N.-M. and D.-K. Lee, *Charged nanoparticles in thin film and nanostructure growth by chemical vapour deposition.* Journal of Physics D: Applied Physics, 2010. **43**(48): p. 3001-3038.

12. Hwang, N.-M., *Non-classical crystallization of thin films and nanostructures in CVD and PVD processes*. Springer Series in Surface Sciences. 2016, Dordrecht: Springer Netherlands. 332.

13. Jung, J.-s. and N.-m. Hwang, *Non-classical crystallization of thin films and nanostructures in CVD process.* Chemical Vapor Deposition: Recent Advances and Applications in Optical, Solar Cells and Solid State Devices, 2016: p. 23.

14. Kim, D.-S. and N.-M. Hwang, *Synthesis of nanostructures using charged nanoparticles spontaneously generated in the gas phase during chemical vapor deposition.* Journal of Physics D: Applied Physics, 2018. **51**(46): p. 3002-3024.

15. Song, J.-H., et al., *Effect of negatively charged species on the growth behavior of silicon films in hot wire chemical vapor deposition.* Thin Solid Films, 2008. **516**(15): p. 5122-5126.

16. Bube, R.H., *Electrons in solids*. An introductory survey. 3rd ed. 1992, London: Academic Press. 85-106.

17. Kim, J.Y., D.Y. Kim, and N.M. Hwang, *Spontaneous generation of negatively charged clusters and their deposition as crystalline films during hot-wire silicon chemical vapor deposition.* Pure and Applied Chemistry, 2006. **78**(9): p. 1715-1722.

18. wilson, C.T.R., *On the Condensation Nuclei Produced in Gases by the Action of Rontgen Rays, Uranium Rays, Ultra-Violet Light, and Other Agents.* Philos. Trans. R. Soc. London, Ser. A, 1899. **192**(9): p. 403-453.

19. Katz, J.L., et al., *Nucleation on photoexcited molecules.* Science, 1977. **196**(4295): p. 1203-5.

20. Lee, J.I. and N.M. Hwang, *Generation of negative-charge carriers in the gas phase and their contribution to the growth of carbon nanotubes during hot-filament chemical vapor deposition.* Carbon, 2008. **46**(12): p. 1588-1592.

21. Hong, J.-S., et al., *In-Situ measurements of charged nanoparticles generated during hot wire chemical vapor deposition of silicon using particle beam mass spectrometer.* Aerosol Science and Technology, 2013. **47**(1): p. 46-51.

22. Hong, J.S., et al., *Real time measurements of charged gas phase nuclei during the deposition of silicon thin films by hot wire chemical vapor deposition.* Current Applied Physics, 2013. **13**(4 SUPPL.2): p. S45-S49.

23. Jeon, I.D., et al., *Detection of large cluster ions by time-of-flight mass*

spectrometry with a conversion dynode. Microchemical Journal, 2001. **70**(3): p. 293-299.

24. Jeon, J.D., et al., *Experimental confirmation of charged carbon clusters in the hot filament diamond reactor.* Journal of Crystal Growth, 2000. **213**(1): p. 79-82.

25. Park, J.-W., K.-S. Kim, and N.-M. Hwang, *Gas phase generation of diamond nanoparticles in the hot filament chemical vapor deposition reactor.* Carbon, 2016. **106**: p. 289-294.

26. Jung, J.-S., et al., *Non-classical crystallization of silicon thin films during hot wire chemical vapor deposition.* Journal of Crystal Growth, 2017. **458**: p. 8-15.

27. Zhiyong, Z., et al., *Epitaxial monocrystalline SiC films grown on Si by HFCVD at 780° C.* Materials Science and Engineering, B: Advanced Functional Solid-State Materials, 2000. **75**(2-3): p. 177-179.

28. Hens, P., et al., *Epitaxial growth of cubic silicon carbide on silicon using hot filament chemical vapor deposition.* Thin Solid Films, 2017. **635**: p. 48-52.

29. Robbins, J. and M. Seman, *Production of bulk silicon carbide with hot-filament chemical vapor deposition*. 2013, BASIC 3C Inc;SiC Systems Inc: US.

30. Van Zeghbroeck, B., H. Robinson, and R.R. Brow. *Hot filament CVD growth of 4H-SiC epitaxial layers*. in *Proceedings of the International Conference on Silicon Carbide and Related Materials 2017*. 2018. Washingtin, DC, U.S.: Trans Tech Publications, Ltd.

31. Ivanov, V.K., et al., *Oriented attachment of particles: 100 years of investigations of non-classical crystal growth.* Russian Chemical Reviews, 2014. **83**(12): p. 1204.

32. Zhang, Q., S.-J. Liu, and S.-H. Yu, *Recent advances in oriented attachment growth and synthesis of functional materials: Concept, evidence, mechanism, and future.* Journal of Materials Chemistry, 2009. **19**(2): p. 191-207.

33. Alivisatos, A.P., *Naturally aligned nanocrystals.* Science, 2000. **289**(5480): p. 736-737.

34. Cölfen, H. and S. Mann, *Higher-order organization by mesoscale self-assembly and transformation of hybrid nanostructures.* Angewandte Chemie International Edition, 2003. **42**(21): p. 2350-2365.

35. Cölfen, H. and A. Markus, *Mesocrystals and nonclassical crystallization*. Mesocrystals and Nonclassical Crystallization. 2008, Chichester, England; Hoboken, NJ: Wiley.

36. Gebauer, D. and H. Cölfen, *Prenucleation clusters and non-classical nucleation.* Nano Today, 2011. **6**(6): p. 564-584.

37. Teng, H.H., *How Ions and Molecules Organize to Form Crystals.* Elements, 2013. **9**(3): p. 189-194.

38. Niederberger, M. and H. Cölfen, *Oriented attachment and mesocrystals: non-classical crystallization mechanisms based on nanoparticle assembly.* Physical Chemistry Chemical Physics, 2006. **8**(28): p. 3271-87.

39. Glasner, A. and J. Kenat, *The crystallization of KCl from aqueous solutions in the presence of lead ions. I. A calorimetric study.* Journal

of Crystal Growth, 1968. **2**(3): p. 119-127.

40. Glasner, A. and S. Skurnik, *A New Mechanism for the Crystallization and Growth of Ionic Crystals, with Special Reference to KCl in the Presence of Pb^{2+}Ions.* Israel Journal of Chemistry 1968. **6**.

41. Glasner, A. and M. Tassa, *The Thermal Effects of Nucleation and Crystallization of KBr and KCl Solutions. II. The Heat Of Nucleation and the Supersaturated Solution.* Israel Journal of Chemistry, 1974. **12**(4): p. 799-816.

42. Glasner, A. and M. Tassa, *The Thermal Effects of Nucleation and Crystallization of KBr and KCL Solutions. III. The Heat of Crystallization and the Co-Precipitation of Lead Ions.* Israel Journal of Chemistry 1974. **12**(4): p. 817-826.

43. Sunagawa, I., *Morphology of Minerals*. 1987, Terra Scientific: Tokyo. 509-587.

44. Sunagawa, I., *Growth and morphology of diamond crystals under stable and metastable conditions.* Journal of Crystal Growth, 1990. **99**(1 -4 pt 2): p. 1156-1161.

45. Cölfen, H. and M. Antonietti, *Mesocrystals and Nonclassical Crystallization*. Mesocrystals and Nonclassical Crystallization. 2008. 1-276.

46. Leite, E.R. and C. Ribeiro, *Crystallization and Growth of Colloidal Nanocrystals*. Crystallization and Growth of Colloidal Nanocrystals. 2012.

47. Wolf, S.E., *Nonclassical crystallization of bivalent metal carbonates*. 2009, Universitätsbibliothek Mainz.

48. Bahrig, L., *Self-assembly and Mesocrystal Formation via Non-classical Crystallisation.* 2014.

49. Yuk, J.M., et al., *High-resolution EM of colloidal nanocrystal growth using graphene liquid cells.* Science, 2012. **335**(6077): p. 61-64.

50. Zheng, H., et al., *Observation of single colloidal platinum nanocrystal growth trajectories.* Science, 2009. **324**(5932): p. 1309-1312.

51. Tang, Z., N.A. Kotov, and M. Giersig, *Spontaneous organization of single CdTe nanoparticles into luminescent nanowires.* Science, 2002. **297**(5579): p. 237-240.

52. Zitoun, D., et al., *Single crystal manganese oxide multipods by oriented attachment.* Journal of the American Chemical Society, 2005. **127**(43): p. 15034-15035.

53. Wen, X., et al., *Dendritic nanostructures of silver: facile synthesis, structural characterizations, and sensing applications.* Langmuir, 2006. **22**(10): p. 4836-42.

54. Liu, J.P., et al., *Self-assembled CuO monocrystalline nanoarchitectures with controlled dimensionality and morphology.* Crystal Growth & Design, 2006. **6**(7): p. 1690-1696.

55. Hwang, N.-M., J. Hahn, and D. Yoon, *Charged cluster model in the low pressure synthesis of diamond.* Journal of Crystal Growth, 1996. **162**(1-2): p. 55-68.

56. Bockris, J.O.M. and A.K.N. Reddy, *Modern Electrochemistry*. Vol. 2. 1970, New York: Plenum.

57. Kumomi, H. and T. Yonehara, *Coarsening Phenomenon of Si Clusters.*

Mater. Res. Soc. Symp. Proc., 1991. **202**: p. 83-88.

58. Cheong, W.S., et al., *Effect of substrates on morphological evolution of a film in the silicon CVD process: approach by charged cluster model.* Journal of Crystal Growth, 2000. **218**(1): p. 27-32.

59. Youn, W.K., et al., *Comparison of the deposition behavior of charged silicon nanoparticles between floating and grounded substrates.* Journal of Physical Chemistry C, 2014. **118**(22): p. 11946-11953.

60. Clare, B.W., et al., *Effect of charge on bond strength in hydrogenated amorphous silicon.* Journal of Computational Chemistry, 1994. **15**(6): p. 644-652.

61. Iijima, S. and T. Ichihashi, *Structural instability of ultrafine particles of metals.* Physical Review Letters, 1986. **56**(6): p. 616-619.

62. Ajayan, P.M. and S. Iijima, *Wetting and de-wetting transitions of small metal particles on substrates under electron irradiation.* Journal of Colloid and Interface Science, 1991. **147**(1): p. 281-285.

63. Takamura, Y., et al., *Cluster size measurement using microtrench in a thermal plasma flash evaporation process.* Journal of Vacuum Science and Technology B: Microelectronics and Nanometer Structures, 1997. **15**(3): p. 558-565.

64. Takamura, Y., et al., *High-rate deposition of $YBa_2Cu_3O_{7-x}$ films by hot cluster epitaxy.* Journal of Applied Physics, 1998. **84**(9): p. 5084-5088.

65. Terashima, K., et al., *High rate deposition of thick epitaxial films by thermal plasma flash evaporation.* Pure and Applied Chemistry, 1998. **70**(6): p. 1193-1197.

66. Hayasaki, K., et al., *Scanning tunneling microscopy of epitaxial $YBa_2Cu_3O_{7-x}$ films prepared by thermal plasma flash evaporation method.* Journal of Applied Physics, 1997. **81**(3): p. 1222-1226.

67. Yamaguchi, N., et al., *Molecular dynamics study of cluster deposition in thermal plasma flash evaporation.* Thin Solid Films, 1999. **345**(1): p. 34-37.

68. Hattori, T., et al., *Deposition of High-Critical-Temperature Superconductor $YBa_2Cu_3O_{7-x}$ Epitaxial Thick Film by Hot Cluster Epitaxy.* JOURNAL-JAPAN INSTITUTE OF METALS, 1999. **63**: p. 68-73.

69. Takagi, T., I. Yamada, and A. Sasaki, *Ionized-cluster beam deposition.* Journal of Vacuum Science and Technology, 1975. **12**(6): p. 1128-1134.

70. Yamada, I., H. Usui, and T. Takagi, *Formation mechanism of large clusters from vaporized solid material.* Journal of Physical Chemistry, 1987. **91**(10): p. 2463-2468.

71. Takagi, T., et al., *Proceedings of the 2nd International Conference on Ion Sources.* 1972.

72. Brown, W., et al., *Ion cluster beam deposition of thin films.* Nuclear Instruments and Methods in Physics Research Section B: Beam Interactions with Materials and Atoms, 1991. **59**: p. 182-189.

73. Yamada, I., H. Inokawa, and T. Takagi, *Epitaxial growth of Al on Si(111) and Si(100) by ionized-cluster beam.* Journal of Applied Physics, 1984. **56**(10): p. 2746-2750.

74. Chung, Y.-B., et al., *Effect of the initial structure on the electrical*

property of crystalline silicon films deposited on glass by hot-wire chemical vapor deposition. Journal of Nanoscience and Nanotechnology, 2012. **12**(7): p. 5947-5951.

75. Iijima, S. *Some experiments on structural instability of small particles of metals*. in *Proceedings of the First NEC Symposium*. 1986. Hakone and Kawasaki, Japan: Springer.

76. Iijima, S. and P.M. Ajayan, *Substrate and size effects on the coalescence of small particles.* Journal of Applied Physics, 1991. **70**(9): p. 5138-5140.

77. Jeon, I.-D., et al., *Effect of methane concentration on size of charged clusters in the hot filament diamond CVD process.* Journal of Crystal Growth, 2001. **223**(1-2): p. 6-14.

78. Lee, S.C., et al., *Effects of cluster size and substrate temperature on the homoepitaxial deposition of Au clusters.* Journal of Crystal Growth, 2002. **242**(3-4): p. 463-470.

79. Menon, P.M., et al., *Filament metal contamination and Raman spectra of hot filament chemical vapor deposited diamond films.* Diamond and Related Materials, 1999. **8**(1): p. 101-109.

국문초록

다양한 분야에서 고효율 및 고성능을 가지는 장치에 대한 요구가 증가함에 따라, 기존의 물질보다 더 우수한 기능과 신뢰성을 가진 물질의 개발이 요구되고 있다. 탄화규소(SiC)는 넓은 밴드 갭, 높은 절연 파괴 전압, 높은 열전도도, 높은 전자 이동도와 같이 우수한 물리적 특성을 가진 물질로써, 이를 전력 반도체, 고효율 LED 디바이스, 태양 전지 등에 적용하기 위해 많은 연구가 활발하게 진행되고 있다.

화학 기상 증착(CVD)은 주로 결정질 SiC을 증착하는데 주로 쓰이는 장비이다. 그중에서도 열선 필라멘트 화학 기상 증착법(HWCVD)은 다른 화학 기상 증착법과 비교하여 저온 증착이나 대면적 증착 낮은 유지비 등의 측면에서 유리하다.

한편으로 결정 성장 분야에서 원자나 분자가 아닌 나노 입자에 의해서 결정이 성장한다고 말하는 비고전적 결정화가 대두되고 있다. 액상에서뿐만 아니라 기상에서도 이에 관한 많은 연구가 진행되고 있다. 많은 결과가 다양한 CVD 공정의 기상에서 하전된 나노 입자가 발생함을 보여주었다.

이러한 이해를 바탕으로 본 연구에서는 HWCVD를 이용한 SiC 필름의 증착 거동을 연구하였다. 먼저, 필름의 성장은 나노 입자에 의해서 이루어지기 때문에 SiC 나노 입자를 셔터를 이용하여 30초간 캡처 후 투과 전자 현미경(TEM)을 이용하여 관찰하였다.

기상에서 하전된 나노 입자의 발생을 확인하기 위해 지연 시간 공정이 도입되었다. SiC 나노 입자의 크기는 지연 시간이 0분부터 60분으로 늘어남에 따라 2.9 nm에서 6.1 nm로 증가하였다. 이는 증착된 나노 입자가 기상에서 유래된 것임을 의미한다.

열선 필라멘트 화학 기상 증착 중 기상에서 생성된 나노 입자들은 하전을 띠고 있기 때문에, 이들의 거동은 전기장에 의해서 영향을 받는다. 기판에 음의 바이어스를 가했을 때는 가하지 않았을 때와 나노 입자의 수가 큰 차이가 없는 반면, 양의 바이어스를 기판에 가했을 때는 SiC 나노 입자의 수가 약간 감소하였다.

하전된 나노 입자 이론에 대한 이해에 따르면, SiC 필름의 증착 거동은 기판에 가한 바이어스에 영향을 받는다. 기판에 - 200 V의 바이어스를 가했을 때 동종 에피택시 SiC 필름이 막의 아래쪽에서 증착되었다. 반면, 바이어스를 걸지 않거나 + 15 V의 바이어스가 기판에 가해졌을 때는 다결정

SiC 필름이 증착되었다. 이러한 기판 바이어스에 따른 필름의 결정성 변화로부터 이는 기상에서 생성된 나노 입자들이 하전되어 있음을 의미한다.

또한, 나노 입자의 거동은 전구체 가스의 농도, 필라멘트 온도 등과 같은 다양한 공정 파라미터에 의존한다. 텅스텐 필라멘트의 온도가 2300℃일 때, 2 ~ 3 nm 크기의 SiC 나노 입자가 캡처되었다. 그러나 필라멘트 온도를 2000℃로 낮추었을 때 약 8 nm 크기의 SiC 나노 입자가 캡처되었다. 전구체 가스의 비인 $(SiH_4 + CH_4)/H_2$을 0.04에서 0.01로 감소시켰을 때 SiC 나노 입자의 크기는 3 nm에서 1 nm로 감소하였다. 입자의 개수 농도 또한 전구체 가스의 농도를 줄임에 따라서 감소하였다.

필라멘트에 추가적인 바이어스를 가함에 따라서 나노 입자의 거동이 어떻게 바뀌는지를 관찰하기 위해서 필라멘트에 + 50 V, 0 V, - 50 V를 걸고 나노 입자를 캡처하였다. 필라멘트에 양의 바이어스를 걸어주었을 때, 나노 입자의 크기 분포에서 바이어스를 걸지 않는 것과 큰 차이가 없었다. 반면, 음의 바이어스를 필라멘트에 가했을 때는 어떠한 나노 입자도 관찰되지 않았다.

비고전적 결정 성장 이론에 따르면 나노 입자의 크기는 그들의 액체와 같은 성질에 영향을 미친다. 나노 입자의 크기가 작으면 액체처럼 행동하

며, 입자의 크기가 클 경우 반대가 된다. 이러한 이해를 바탕으로 하전된 나노 입자의 거동을 제어함으로써 동종 에피택셜 SiC 필름을 증착할 수 있는지 확인하였다. 나노 입자의 크기가 충분히 작을 때, 약 100 nm 두께의 동종 에피택시 필름이 증착되었다. 나노 입자의 크기가 클 때에는 다결정 SiC 필름이 증착되었다.

이 연구를 통해서 얻은 결과들은 기상에서 생성된 나노 입자의 크기와 하전이 필름 성장에 있어서 중요한 역할을 함을 보여주는 중요한 실험적 증거가 될 수 있다.

핵심어: 탄화 규소, 열선 필라멘트 화학 기상 증착, 비고전적 결정 성장, 박막 성장, 4H-탄화규소

학번: 2013-23035